Metals and Ceramics Division

Heavy Vehicle Propulsion Materials Program
Quarterly Progress Report for
October through December 2000

D. R. Johnson
Technical Project Manager

Prepared for
U.S. Department of Energy
Assistant Secretary for Energy Efficiency and Renewable Energy
Office of Transportation Technologies
EE 07 01 00 0

Prepared by the
OAK RIDGE NATIONAL LABORATORY
Oak Ridge, Tennessee 37831-6066
Managed by
UT-Battelle, LLC
for the Department of Energy
Under contract DE-AC05-00OR22725

CONTENTS

Cost Effective High Performance Materials and Processing

Development of Low Cost Austenitic Stainless Diesel Engine Components with Enhanced High-Temperature Reliability (ORNL and Caterpillar, Inc.)

Development of NOx Sensors for Heavy Vehicle Applications (ORNL, Ford Motor Company, and Visteon Automotive Systems)

Cost-Effective Smart Materials for Diesel Engine Applications (ORNL)

Low-Cost Manufacturing Processes for Ceramic and Cermet Diesel Engine Components (SIU-C)

Low Cost High Toughness Ceramics (ORNL)

Advanced Manufacturing Technology

Intermetallic-Bonded Cermets (ORNL)

Low-Cost Manufacturing of Precision Diesel Engine Components (ORNL)

Cylindrical Wire Electrical Discharge Machining (EDM) and Temperature Measurement (North Carolina State University)

Testing and Characterization

NDE Technology for Heavy Duty Diesel Engines: Fuel Delivery and Insulating Materials (Argonne National Laboratory)

NDE Development for Ceramic Valves for Diesel Engines (Argonne National Laboratory)

Processing and Characterization of Structural and Functional Materials for Heavy Vehicle Applications (North Carolina A&T State University)

Life Prediction of Diesel Engine Components (ORNL)

Field Emission Analytical Electron Microscopy for Characterization of Catalyst Microstructures (ORNL)

Durability of Diesel Engine Component Materials (ORNL)

Materials and Testing Standards

Implementing Agreement for a Programme of Research and Development on Advanced Materials for Transportation Applications (ORNL)

Standards for Reliability Testing of Heavy Vehicle Propulsion Materials (NIST)

Mechanical Property Testing and Standards Development (NIST)

Development Of Low-Cost Austenitic Stainless Diesel Engine Components With Enhanced High-Temperature Reliability

P.J. Maziasz and R.W. Swindeman
Oak Ridge National Laboratory
and
C.W. Siebenaler and M.T. Kiser
Caterpillar, Inc.

Objective/Scope

The objective of this work is to evaluate cast austenitic stainless steels as alternate materials for SiMo ductile cast iron, which is currently used in most diesel engines for exhaust manifold and turbocharger housing components. Any new material must be able to withstand prolonged exposure at temperatures of 750°C or above, as well as survive the severe thermal cycling from near room temperature to such high temperatures without developing cracks. This project has tested commercially available cast alloys, as well as developed new, modified cast alloys with significantly enhanced performance. The ultimate goal is to provide a high-performance, reliable material that is also cost-effective for such applications. This advanced diesel engine work is part of a larger CRADA (Cooperative Research and Development Agreement) project (ORNL99-0533) that began July 21,1999, and will last 2 years. The large CRADA project is blended achieve similar objects for advanced gas-turbine engines as well as advanced diesel engines. More detailed information must be requested directly from Caterpillar, Inc.

Technical Highlights, 1st Quarter, FY 2001

Background

Advanced large diesel engines must have higher fuel efficiency as well as reduced exhaust emissions. Therefore, exhaust manifold and turbocharger housing materials must withstand temperatures ranging from 70 to 750°C or higher in a normal duty cycle that includes prolonged, steady high-temperature exposure as well as more rapid thermal cycling. New technology like exhaust gas recirculation (EGR) to reduce emissions will likely push temperatures in these critical components even higher. Current materials such as SiMo ductile cast iron would be pushed beyond their strength and corrosion limits, so new materials like cast austenitic stainless steels must be considered. Currently, there is little industrial experience or appropriate high-temperature mechanical properties data available on cast austenitic stainless steels, like CN12, particularly for diesel engine applications. The purpose of this program is to focus on the exhaust manifold component and produce data on cast CN12 and compare it to SiMo cast iron for such diesel component applications.

Approach

Commercial cast CN12 austenitic stainless steel (Fe-25Cr-13Ni-1.8Nb,C,N) was chosen as the baseline alloy for evaluation relative to SiMo ductile cast iron. Materials were evaluated in

the as-cast condition as well as after appropriate thermal aging at temperatures up to 850°C. Tensile and cyclic isothermal fatigue properties were evaluated selectively from room temperature up to 900°C, together with some high-temperature creep-rupture and oxidation/corrosion testing. Microstructural analysis was performed on some of the specimens to better understand mechanisms associated with the properties changes. In parallel, alloy modifications to CN12 were also studied to further enhance the high-temperature performance.

Technical Progress

To date, the commercial cast iron and baseline CN12 materials have been obtained, all mechanical properties specimens machined, and all tensile and creep testing of unaged and aged specimens has been done. High-cycle isothermal fatigue up to 700°C has been completed, and similar fatigue testing at higher temperatures or thermal fatigue over this temperature range are in progress or remain to be done. Microstructural analysis of selected specimens has been completed or is in progress to understand the properties behavior and to establish the effects of aging on the baseline CN12 material.

To date, eight smaller heats (15 lbs each) of modified CN12 austenitic stainless steels have been produced at ORNL and have been evaluated. Preliminary screening of as-cast or aged material with tensile testing, and of as-cast material with creep-rupture testing at 850°C indicates that significant improvements have been achieved in high-temperature strength and aging resistance.

Communications/Visits/Travel

Team communications between ORNL and Caterpillar occur on a regular basis. As part of the user-agreements imbedded in the CRADA, Mike Pollard of Caterpillar worked for 1 week at ORNL in January 2000, and Tim McGreevy (formerly at Caterpillar and now at Bradley University) worked for 2 weeks at ORNL in June 2000. Phil Maziasz of ORNL visited the Caterpillar Technical Center in Mossville, IL, for technical discussions and to summarize the progress of this project.

During this last quarter, preparation of an invention disclosure and patent application on cast austenitic stainless alloys with improved performance began at Caterpillar.

Status of Milestones

Formal milestones are imbedded in the CRADA and are not part of the HVPM Program FWP. However, all milestones have been achieved on or significantly ahead of schedule.

Publications

None.

Development of NOx Sensors for Heavy Vehicle Applications

Timothy A. Armstrong
Oak Ridge National Laboratory

CRADA No. ORNL99-0566
with Ford Motor Company and Visteon Automotive Systems

Objective

This project is developing novel materials for use in NOx sensors and test methods to enhance the signal output from NOx sensors based on pumping cell technology.

Results

Sensor response was measured for gas temperatures of 27°C and approximately 188°C. The response times for the sensor at these two conditions are shown in Table 1.

Table 1. Sensor response results

	Gas temperature = 27°C	Gas temperature = ~188°C
RC Time Constant	1.67	1.18
t(10-90)	3.6 s	2.6 s
t(33-66)	1.13 s	0.8 s

The sensor response was faster for the test performed at 188°C than for the one performed at room temperature (27°C). These results show that response increases with temperature. This is not surprising when you consider that the test gas may lower the temperature on the electrolyte surface by convection. This drop in temperature is probably significant enough to reduce oxygen diffusion through the electrolyte, thereby increasing the response time of the sensor.

Also, during this quarter a novel substrate composition was developed that increased its fundamental resistivity at 800°C to greater than 5 MΩ. This composition is currently being scaled up for testing with our industrial partner.

Cost-Effective Smart Materials for Diesel Engine Applications

J. O. Kiggans, Jr., T. N. Tiegs, F. C. Montgomery
and L. C. Maxey
Oak Ridge National Laboratory

Objective / Scope

There are two objectives for this project. The first is to evaluate the cost-effectiveness and maturity of various "Smart Materials Technologies," which are under consideration for diesel engine applications, such as fuel injection systems. The second is to develop "Smart Materials" to be incorporated into working actuators and sensors.

Task 1 - Multilayer Electroded Laminates

The purpose of this study is to find satisfactory methods for the preparation of PZT laminates with internal electrodes from tape cast materials. This task is in progress with no results to share in this report.

Task 2 – Compositional Alteration of PZT-4

A second task of this project is the study of cost-effective alternative PZT compositions and processing methods which will allow low temperature (<1125°C) sintering. Various sintering additives were selected for this study based on literature references.

Two basic commercial powders were used to make standard (non-doped) samples for this study: 1) APC 840 (American Piezo Ceramics Inc.) also designated PZT-4 and 2) TRS 200FG (TRS Ceramics, Inc). The APC 840 is a "hard" composition that we have used for several previous studies. The TRS 200FG is a new fine-grained soft PZT powder that was developed for higher sintered strength due to its fine grain size. Several compositions of APC 840 material with ceramic additives were fabricated for this study. Previous studies in our laboratories and others have shown that bismuth oxide additions to PZT can lower the sintering temperature and, in most cases, increase the piezoelectric d_{33} coefficient of the materials. Although bismuth has been shown to react with palladium in electrode materials, the bismuth solid solutions fabricated in this study may be less reactive to electrode materials.[1,2,3,4] Zirconium tungstate was also used as an additive because it has a negative expansion coefficient and thus may increase the sintered strength.

Methods for sample preparation were described in previous reports. Final sintering temperatures were 893°, 960°, 1025°, and 1125°C. Following sintering runs, all samples were weighed and the weight change calculated, and the densities were measured. The sample discs were then ground, and silver electrodes were applied to each side using previously described procedures. The samples were then poled, and the electromechanical properties measured. The samples were ground again to remove the electrodes and polished. Samples were etched for 5 to 120 s at room temperature with a solution containing 2.3 wt. % hydrochloric acid and 0.12 wt. % hydrofluoric acid. A part of each polished disc was broken to create a fracture surface for viewing. Polished and fracture surfaces of PZT samples were coated with either carbon or gold prior to SEM analysis.

Table 1 lists the sintered densities and the d_{33} coefficients of the various sample types fabricated for this study. Some of this data has appeared in previous reports, but is presented here as a reference for discussions comparing the relationships of the densities and d_{33} coefficients with the microstructures as evaluated with the SEM. Figure 1 shows the SEM images of the fracture and polished surfaces of control APC 840 and the TRS 200FG materials sintered at 1125°C. The sintered densities of these samples were 98.0% and 100.8% T. D., respectively. The TRS material had a finer average grain size, less than 2 µm diameter, than the APC material which had a large number of grains around 2 µm. As a soft material, the TRS had a higher d_{33} coefficient, 0.43 compared to 0.27 value for the APC 840 material. The high densities and d_{33} coefficients make both materials candidates for use with silver–palladium electrodes in multilayer devices. Figure 2 shows SEM images of APC 840 materials containing sintering additives, which were sintered at 1125°C. Figure 2 (top) are fracture and polished images of APC 840 material containing 2 wt. % bismuth oxide. This sample reached a density of 100.9 % T. D. and had a d_{33} coefficient of 0.38. The bismuth addition resulted in large grain growth in some grains, with grain sizes ranging from 1 to 20 µm in diameter. It appears that most of the larger grains in this material exhibit a transgranular fracture mode. It is thought that this larger average grain diameter may lead to lower strengths, but testing will be necessary to prove this point. Figure 2 (middle) show images of APC 840 material containing 2 wt. % bismuth titanate. This material sintered to a density of 99.3 % T. D., and the d_{33} coefficient was 0.32. The polished image shows grains varying in size from 0.5 to 5 µm in diameter. The fracture surface shows numerous small grains, which appear to have pulled out from larger grains during the sample polishing process. One such small grain is seen at the intersection of a number of larger grains in the image of the polished surface (arrow). Figure 2 (bottom) show images of APC 840 material containing 2 wt. % zirconium tungstate. This material sintered to a density of 101.4% T.D, and the d_{33} coefficient was 0.35. This microstucture is very different from the other materials tested with grains varied in size from 0.2 to 3 µm in diameter. As with the materials, which contained bismuth titanate, this sample has a significant number of small particles. It will be interesting to see if these small particles offer any strength enhancement.

Figure 3 shows SEM images of PZT materials sintered at 1025°C. Figure 3 (top) shows images of TRSFG material. This material sintered to a density of 91.7% T.D, and the d_{33} coefficient was 0.26. Both of these two properties rule out this sintering temperature. The polished image shows grains varying in size from 0.2 to 1µm in diameter. The fracture surface of this material is very irregular with no good delineation of fracture surfaces. Figure 3 (middle) shows images of APC 840 material with 2 wt. % $Bi_2Cu_{0.1}V_{0.9}O_{5.35}$ additive. This material sintered to a density of 99.3% T.D, and d_{33} coefficient was 0.32. The polished image shows grains varying in size from 1 to 10 µm in diameter. The fracture surface shows both intergranular and transgranular fracture. Figure 3 (bottom) shows images of APC 840 material with 2 wt. % ZrW_2O_8 additive. This material sintered to a density of 88.6% T.D, and d_{33} coefficient was 0.05. Again, these lower properties rule out this sintering temperature. The fracture image shows rounded grains of undetermined diameters. Numerous attempts were made to obtain a good polished image with no success.

Figures 4 and 5 show SEM images of PZT materials sintered at 893°C. Figure 4 (top) shows images of APC 840 material containing 2 wt. % bismuth oxide. This material sintered to a

density of 100.5% T.D, and d_{33} coefficient was 0.35. The polished image shows grains varying in size from 1 to 3 µm in diameter. The fracture surface shows that there was primarily intergranular fracture. An additional batch of this material type was made that yielded a very different result. This material sintered to a density of 84.6% T. D., and the d_{33} coefficients was only 0.11. The polish surface was difficult to obtain, similar to other PZT samples, which did not reach >90 % sintered densities. X-ray analysis is being conducted to determine if the compositions are grossly different between the two powder batches. Figure 5 shows SEM images of three other powders fabricated from APC 840 material containing sintering additives that were sintered at 893°C. Figure 5 (top) images are of APC 840 material containing 2 wt. % $65Bi_2O_3$-6CuO-$29V_2O_5$. This material sintered to a density of 100.3% T.D, and the d_{33} coefficient was 0.32. The polished image shows grains varied in size from 0.5 to 3 µm in diameter. The fracture surface shows that both intergranular and transgranular fracture mode. Figure 5 (middle) images were of APC 840 material containing 2 wt. % $Bi_2Cu_{0.1}V_{0.9}O_{5.35}$. This material sintered to a density of 96.8% T.D, and d_{33} coefficient was 0.28. The polished image shows grains varying in size from 1 to 3 µm in diameter. The fracture surface image shows both intergranular and transgranular fracture mode. Figure 5 (bottom) images are of APC 840 material containing 2 wt. % $31Bi_22O_3$-44SrO-25Cu. This material sintered to a density of 99.0% T.D, and d_{33} coefficient was 0.32. The polished image shows grains varying in size from 1 to 3µm in diameter. The fracture surface shows both intergranular and transgranular fracture mode. Samples these bismuth oxide–based compositions will be tested for interactions with Ag and Ag-Pd electrode materials.

Task 3 - Mechanically Amplified Piezo-Actuator System

Conventional piezoelectric stack actuators with moderate dimensions desired for fuel injector drivers (~2.05 cm diameter by ~5 cm long) can be fabricated to produce tremendous forces (> 150 kg), but are often limited to very small displacements (< 25 µm). To achieve larger displacements, the length of the actuator must be increased. This increase in actuator length will increase the capacitance of the device, which can impose additional demands on the power electronics necessary to drive the actuator.

An intuitive approach to tailoring the performance characteristics to a given application is to use a smaller physical actuator and convert some of the piezoelectric force into displacement through a mechanical amplifier. The challenges of implementing this approach, however, are quite complex due to the small initial displacement. The material modulus, manufacturing methods, surface finishes, actuator pre-load and other considerations must be coupled into the design along with the fundamental force and displacement requirements.

A preliminary design of an amplified piezo-actuator system has been developed based on generic fuel injector displacement and force requirements. A prototype will be constructed and evaluated to compare the ultimate performance with the design parameters. A force of 22.5 kg and a displacement of 125µ were selected as the design targets. A small (2.5 cm long x 0.95 cm diameter) stack actuator capable of delivering a 25-µm displacement at approximately 120 kg was selected for use with a nominal 5.9:1 mechanical amplifier. The mechanical amplifier was designed as a monolithic two-stage cantilevered flexure with a passive stabilizer output. Finite

element modeling was performed using Cosmos-M, to arrive at the physical dimensions and pre-load conditions necessary to achieve the design target parameters. The overall piezo-actuator system package dimensions are defined by the amplifier and are approximately 6.7 cm length by 3.3 cm width and 1.25 cm thickness. Drawings will be provided in future reports after fabrication of the amplifier assembly is completed.

Status of Milestones

1) Evaluate and characterize commercially -available PZT materials. Seek methods to improve the properties of these materials through alternative processing and forming methods. Fabricate new PZT compositions that allow sintering of the PZT materials at lower temperatures.
   Status: Both the evaluation of new commercial materials and low temperature PZT materials are in progress.
2) Initiate studies on important variables in the fabrication of multilayer co-fired PZT stacks. Fabricate multilayer PZT stacks for testing.
   Status: PZT tapes have been fabricated and have been printed with silver palladium ink. Co-fire studies are presently in progress.
3) Use ORNL expertise in motion amplifier devices to design and fabricate motion-amplifying fixtures for fuel injector assemblies.
   Status: An amplifier fixture has been designed at ORNL. Final drawings are under review prior to fabrication.

Communications/Travel/Visits

Dr. Paul Becher was the host at ORNL for a visit by M. J. Hoffman of the University of Karlsruhe, Germany. Two meetings were held in which Dr. Hoffman presented recent research results for PZT research and applications for diesel engines in Europe.

Publications

None

References

1. S. F. Wang and J. P. Dougherty, “Silver Palladium Thick Film Conductors,”J. Am. Ceram. Soc., Vol. 77, No. 12, 3051-71, 1994.
2. S. F. Wang and W. Huebner, “Interaction of Ag/Pd Metallization with Lead and Bismuth Oxide-Based Fluxes in Multilayer Ceramic Capacitors,” J. Am. Ceram. Soc., Vol. 75, No. 9, 2339-52, 1992.
3. T. Garino and M. Rodriguez, “Behavior of Silver and Palladium Mixtures during Heating,” J. Am. Ceram. Soc., Vol. 83, No. 11, 2709-14, 2000.
4. M. Valant and D. Suvorov, “Chemical Compatibility between Silver Electrodes and Low-Firing Binary-Oxide Compounds: Conceptual Study,” J. Am. Ceram. Soc., Vol. 83, No. 11, 2721-29, 2000.

Table 1. Sintered density and d_{33} values for PZT compositions sintered at various temperatures

		Density* and d_{33}**values		
Base Powder	Additive - 2 Wt%	893 ^{o}C no atm. powder	1025 ^{o}C	1125 ^{o}C
TRS200FG*	none		91.7% (0.26)	100.8% (0.43)
APC840	none			98.0% (0.27)
APC840	ZrW_2O_8		88.6% (0.05)	101.4% (0.35)
APC840	$Bi_4Ti_3O_{12}$			99.3% (0.32)
APC840	Bi_2O_3	100.5% (0.35)		100.9% (0.38)
APC840	Bi_2O_3	84.64% (0.11)		
APC840	$31Bi_2O_3$-44SrO-25CuO	99.0% (0.32)		
APC840	$Bi_2Cu_{0.1}V_{0.9}O_{5.35}$	96.8% (0.28)	99.3% (0.32)	98.4% (0.36)
APC840	$65Bi_2O_3$-6CuO-$29V_2O_5$	100.3% (0.32)		

*% theoretical density
**x10^{-12} m/V

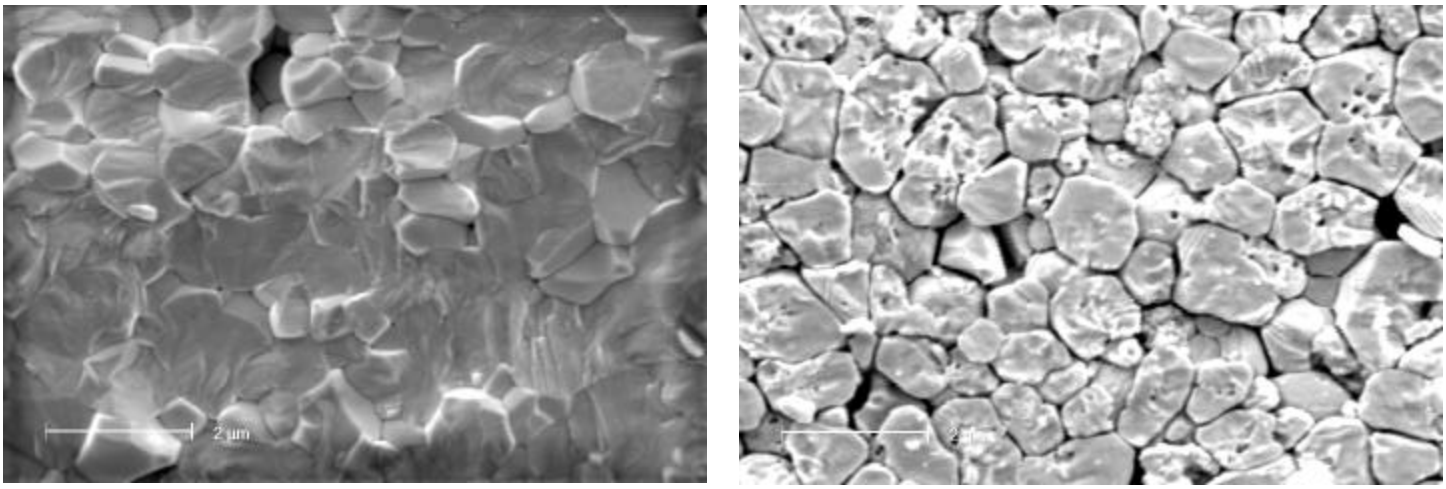

APC 840 PZT-4 1125°C (214a)

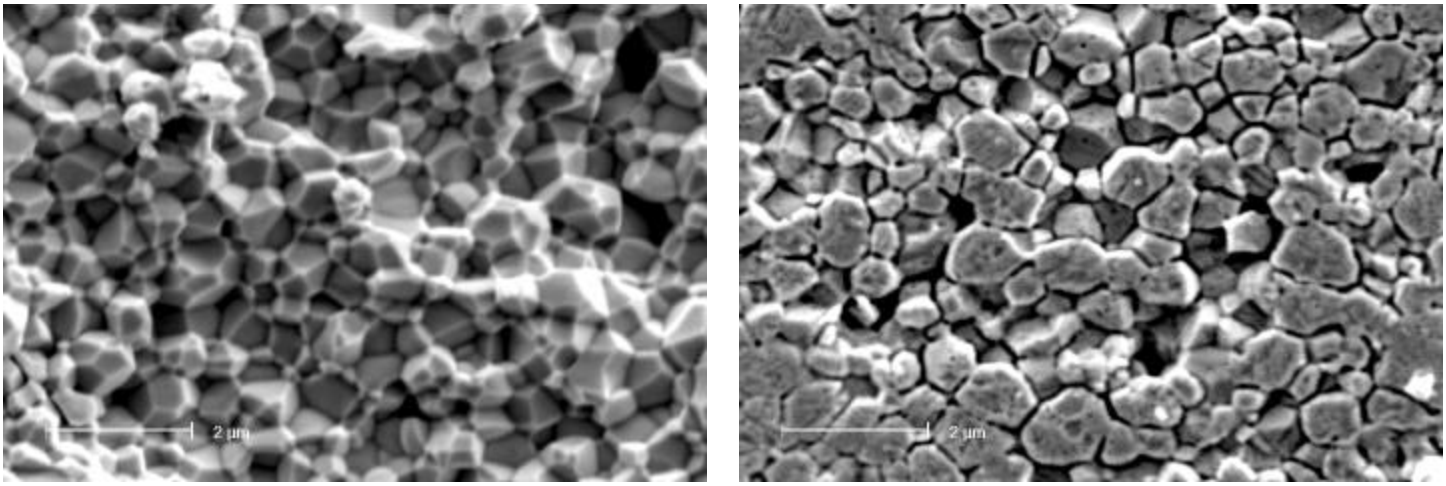

TRS 200FG 1125°C (67G)

Figure 1. SEM images of PZT materials sintered at 1125°C.

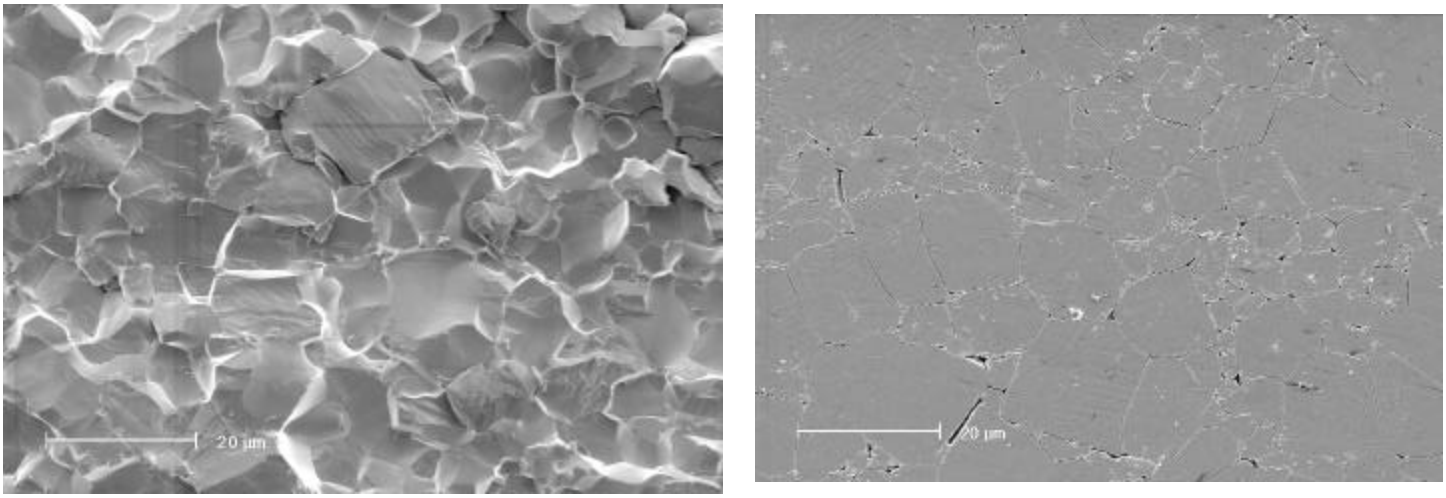

APC 840 + 2 wt % Bi_2O_3 1125°C (214K)

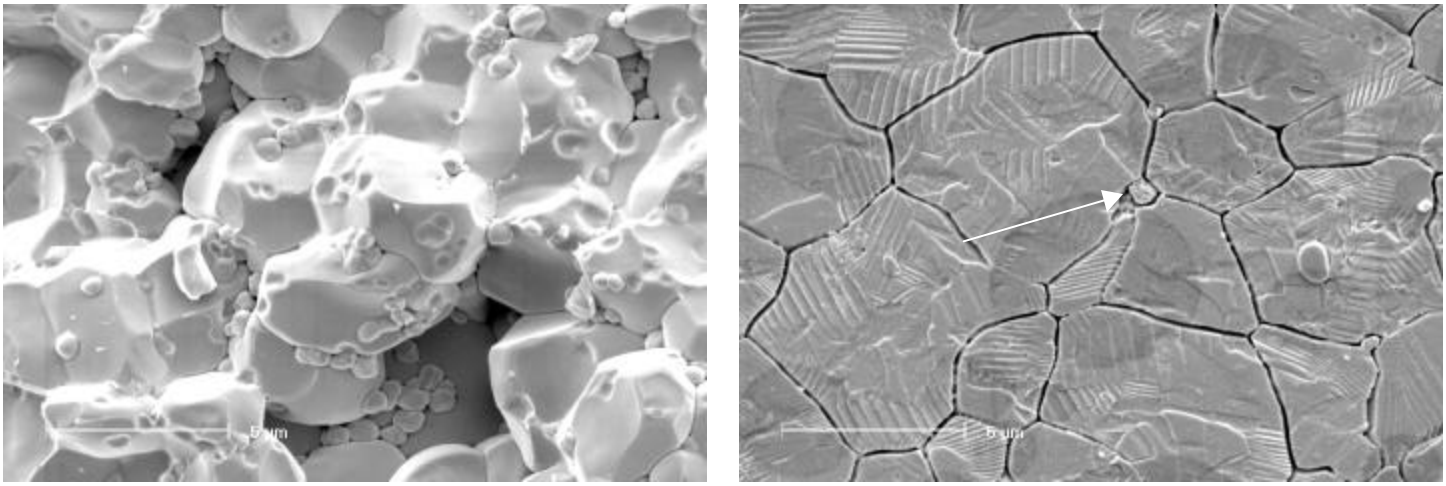

APC 840 + 2 wt % $Bi_4Ti_3O_{12}$ 1125°C (280a)

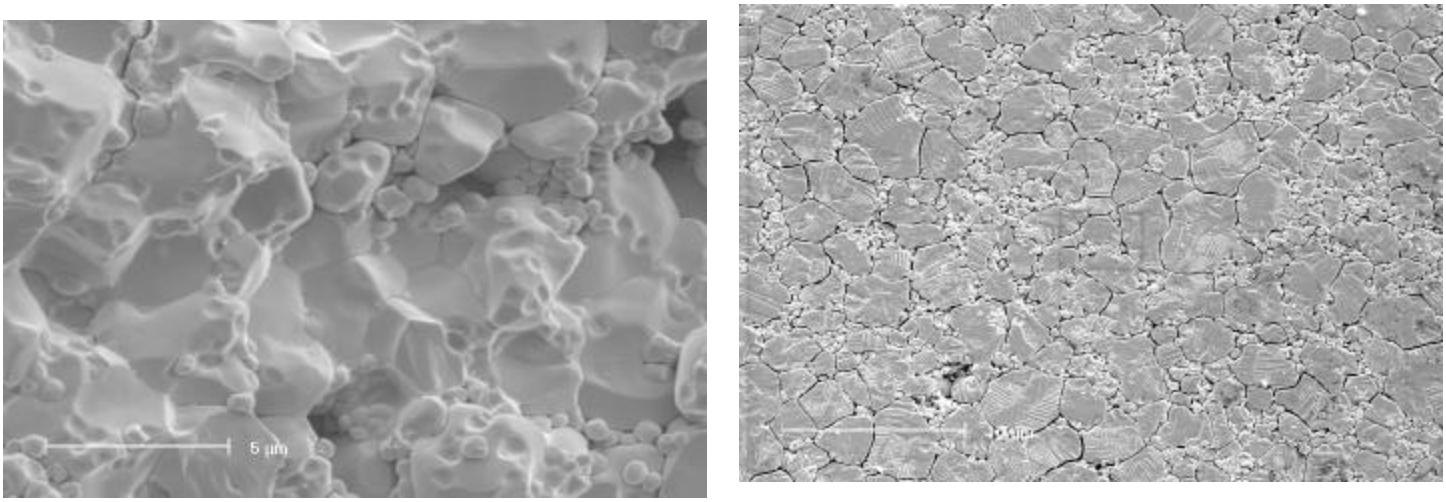

APC 840 + 2 wt % ZrW_2O_8 1125°C (67c)

Figure 2. SEM images of PZT materials sintered at 1125°C.

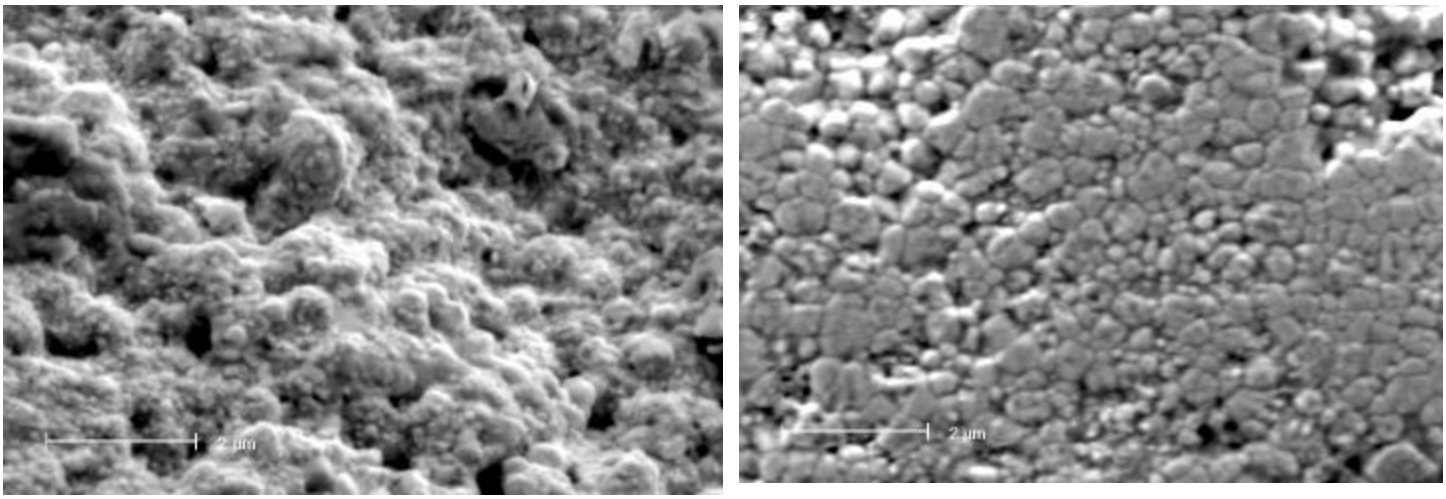

TRS 200FG 1025C(86d)

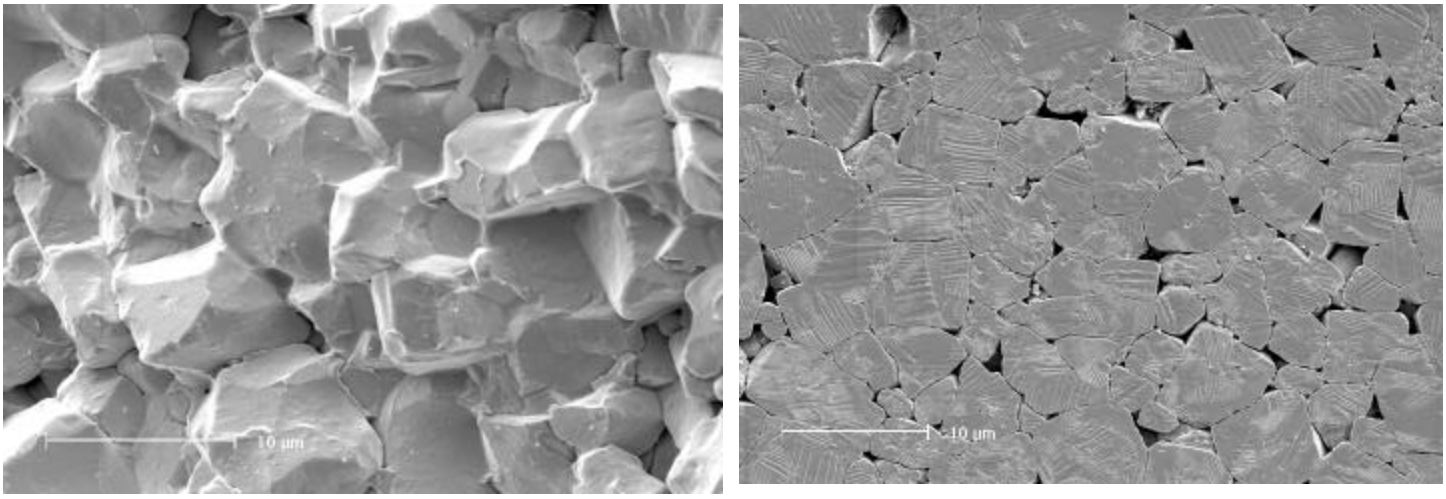

APC 840 + 2 wt % $Bi_2Cu_{0.1}V_{0.9}O_{5.35}$ 1025°C (86F)

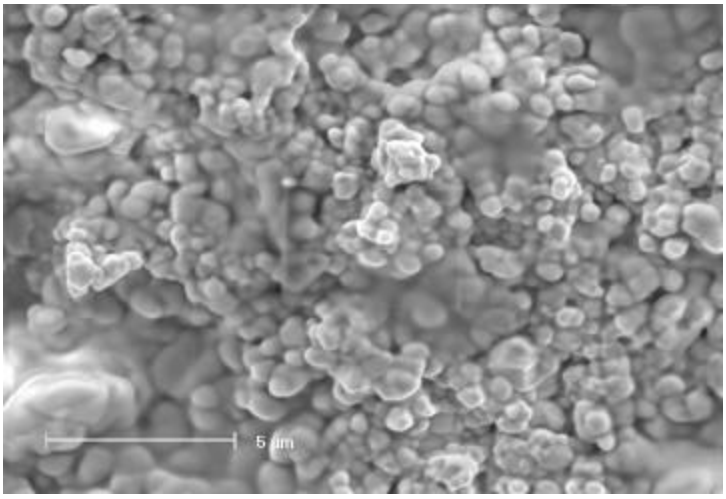

APC 840 + 2 wt % ZrW_2O_8 1025C (86a)

Figure 3. SEM images of PZT materials sintered at 1025°C.

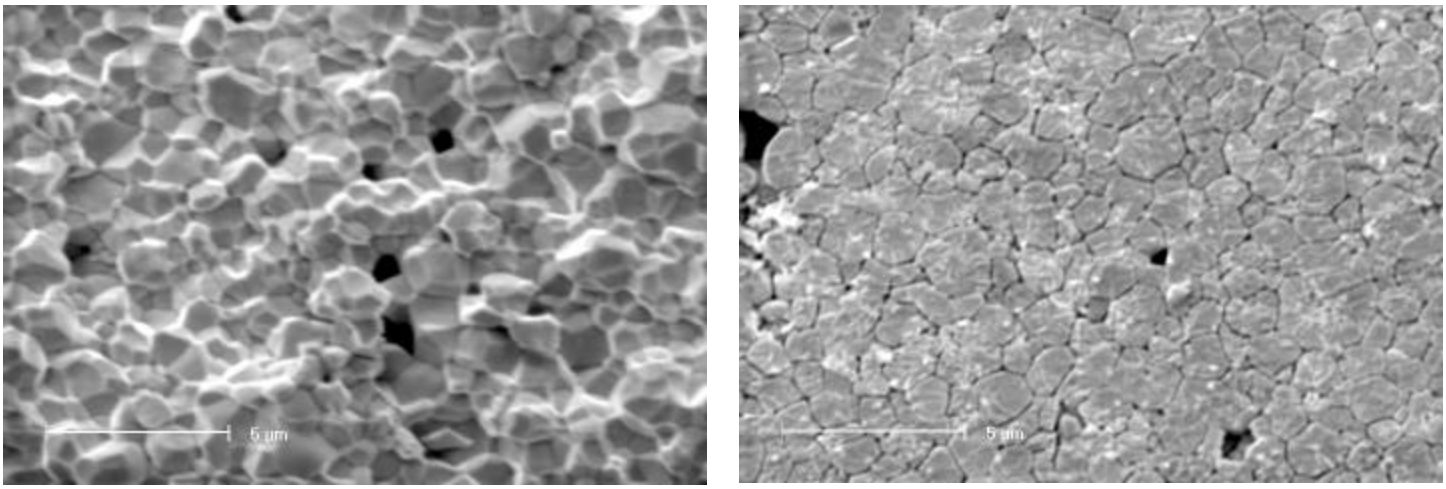

Bi_2O_3 - 893°C (33e)

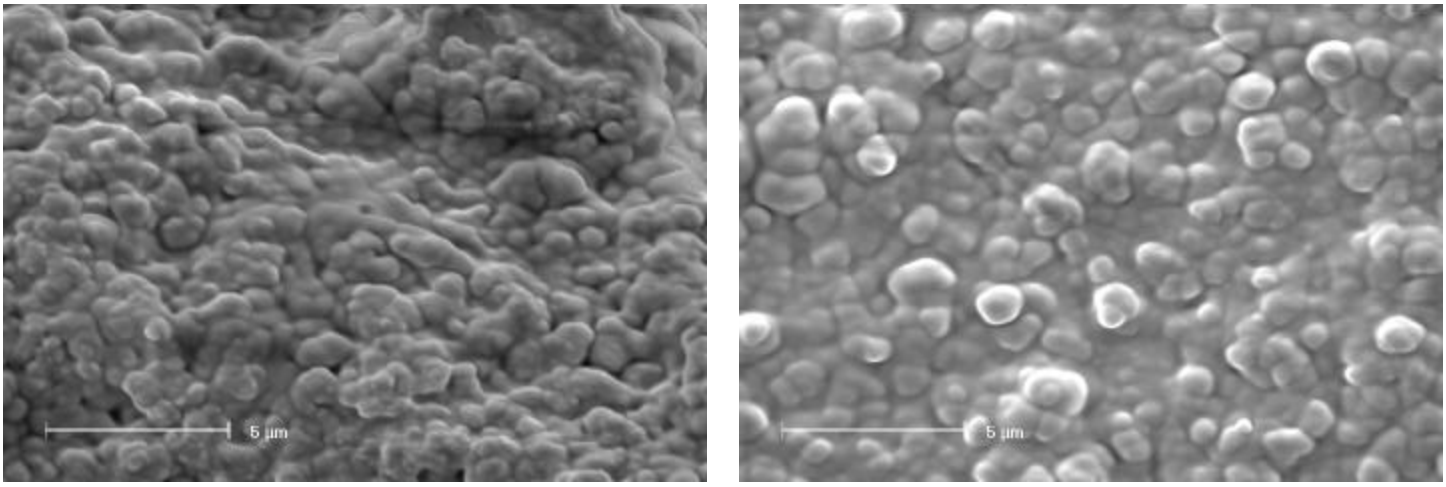

Bi_2O_3 - 893°C (125b)

Figure 4. SEM images of PZT materials sintered at 893°C.

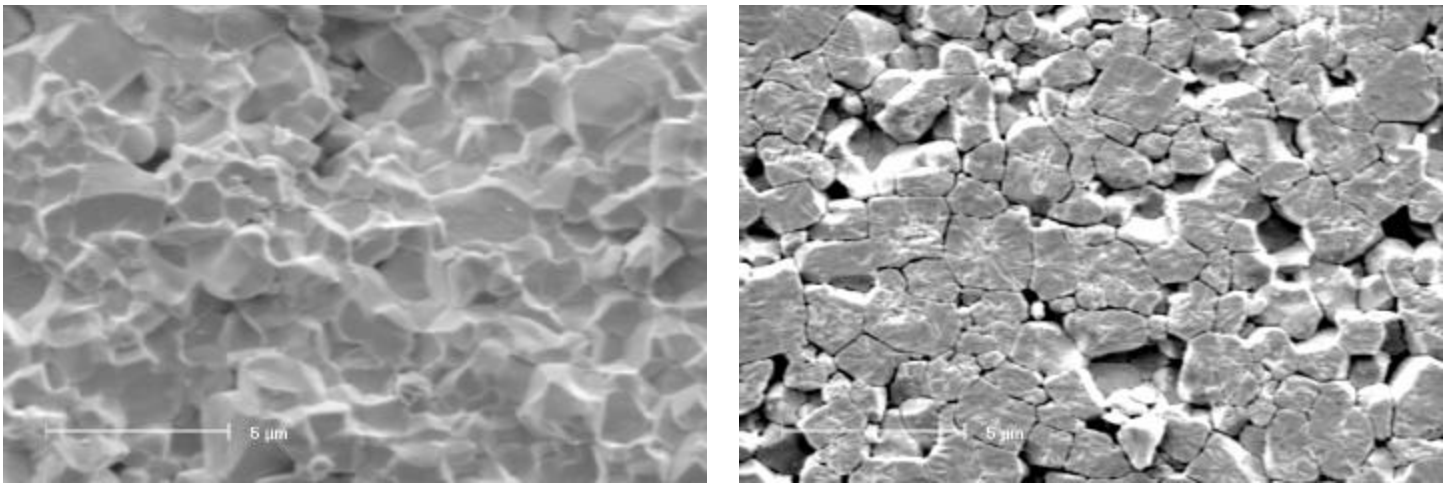

$65Bi_2O_3$-6CuO-$29V_2O_5$ - 893°C (33a)

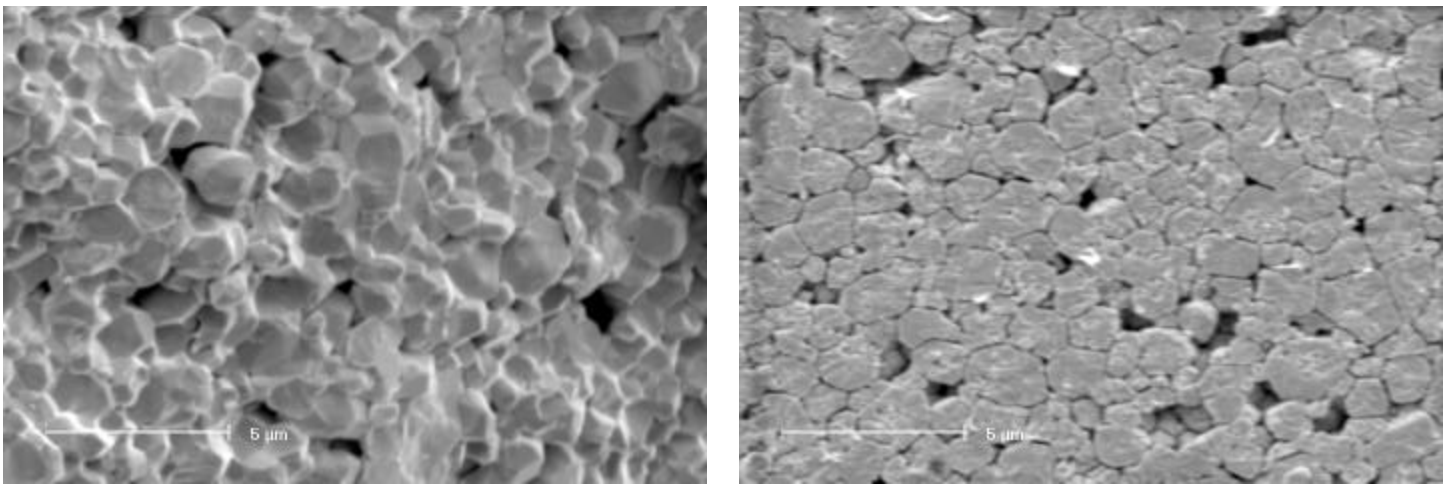

$Bi_2Cu_{0.1}V_{0.9}O_{5.35}$- 893°C (147a)

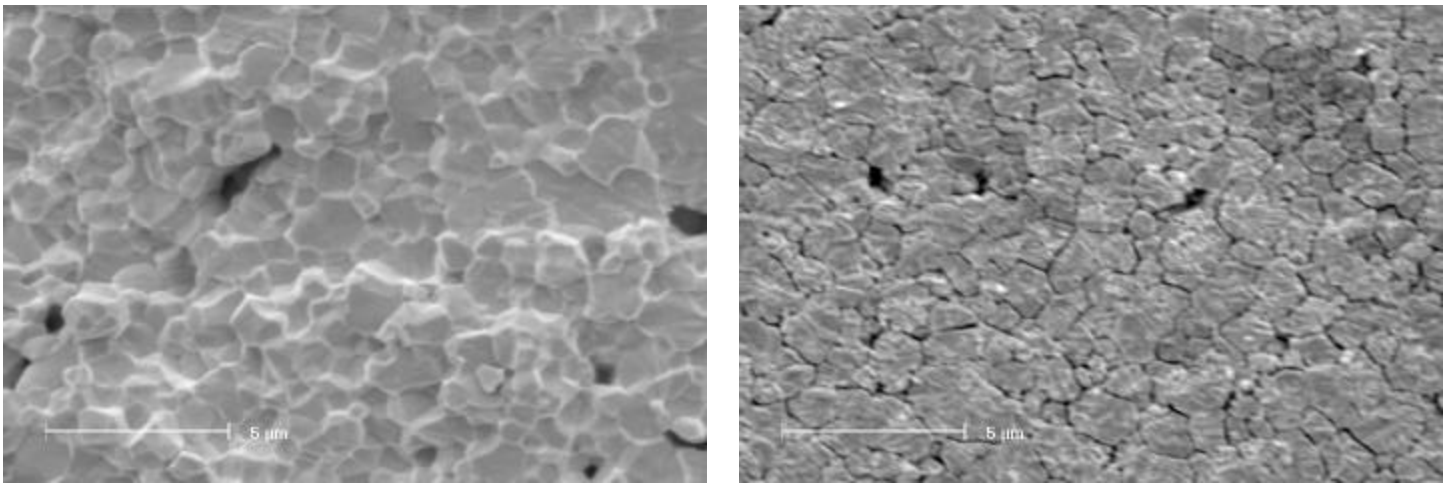

$31Bi_2O_3$-44SrO-25Cu - 893°C (33d)

Figure 5. SEM images of PZT materials sintered at 893°C.

Low-Cost Manufacturing Processes for Ceramic and Cermet Diesel Engine Components

D. E. Wittmer
Department of Mechanical Engineering
and Energy Processes
Southern Illinois University
Carbondale, IL 62901

Objective/Scope

The purpose of this work is to investigate the potential of cost effective sintering of Si_3N_4 and inter-metallic bonded carbides through the development of continuous sintering techniques.

Technical Highlights

Task 1. Refine Economic Model and Design for Chosen Furnace Configuration

This task was completed as reported in a previous semiannual report.

Task 2. Continue evaluation of sintering parameters on properties of selected Si_3N_4 compositions

1. Prototype Belt Furnace

The furnace continues to operate efficiently without problem.

2. Collaboration with Industrial Partners and Affiliates

Work continues according to plan to develop collaborations with industrial partners. Due to the proprietary/confidential relationships established, the results of these collaborations will be reported as part of their individual programs.

3. Evaluation of Continuous Sintering of Silicon Nitride-Titanium Carbide

This task has been completed.

Task 3. Continue Evaluation of Low Cost Si_3N_4 Powders

This task has been completed.

Task 4. Design and Construct Prototype Belt Furnace

This task has been completed.

Task 5. Continuous Sintering of Intermetallic Bonded Carbides

As previously reported, several batches of NiCr and NiCrFe-bonded TiC batches have been ball milled and attritor milled at ORNL and processed in the turbomill at SIU. For ball milling, 13 mm YTZ media were used and milling took place for 24 hours in alcohol. For attritor milling, 1.1 mm WC media were used and milling took place in alcohol at 550 rpm for 4 hours. For turbomilling the TiC was turbomilled for 5.5 hours in isopropanol at 1200 rpm, the intermetallic powders were then added and milling continued for 0.5 hours.

Previously it was reported that turbomilling produced the highest densities and the lowest hardness, which is contrary to expectations, based on density alone. The results for the NiCrFe-TiC composites are given in Figures 1 through 4, while some of the corresponding microstructures are given in Figures 5 through 8.

Figure 1shows that in general the ball mill and attritor mill produced the highest densities for continuous sintering at 1450EC in Ar at a belt speed of 1.5"/min. As with earlier results the hardness values obtained were lower for the turbomilled composites compared with those processed by ball milling or attritor milling (Figure 2).

In an attempt to study the effect of minimal milling on the batching process, the same components for the 40 vol% NiCrFe-TiC formulation were placed in a polypropylene jar and hand shaken for a couple of minutes. Disks were then pressed from the dried powder as in previous experiments. The results are given in Figures 3 and 4 as the non-milled bar, compared with the other processing techniques. As seen the density was equivalent to that obtained for the attritor mill process while the hardness was similar that obtained for the ball mill process. The SEM photomicrographs, Figures 5 through 8 illustrate why the hardness was lower for the turbomilled and ball milled processes and higher for the attritor process. The turbomill process produced microstructures with very large areas of intermetallic, while the attritor mill process appears to have produced a much finer TiC grain size. This makes it affected to a lesser extent by the isolated intermetallic areas. The ball mill and non-milled processes have similar microstructures in that the TiC grain size is similar and the intermetallic areas are small and fewer in number. Further study of these relationships is required.

Low Pressure Injection Molding

During this reporting period, several addition batches of 40 vol% NiCrFe-TiC were processed and injected using the Peltzman MIGL-28 unit. The binder formulation and the injection process has been continually modified in an attempt to reduce/eliminate the defects previously observed. The recent results are given in Table 1.

Table 1. Recent results from injection molding trials.

Sample ID	Organic Binder Vol%	Bisque Density % TD	Batch Sintered Density %TD		Belt Sintered Density %TD	
IM-19	37	64.3	No Iso	Iso	No Iso	Iso
IM-20	34	--	98.8	99.4	91.2	96.0
IM-21	32	--	–	–	–	--
IM-22	35	Blistered	–	–	–	--

All of the mixtures were process as follows: binders were melted in the pre-heated well, the ceramic and metallic powders were then added, mixed with a spatula until the powders were coated (~10 min), the cover was placed on the unit, the mixture was then mixed under vacuum for 60 min. For IM-19 the binder was petroleum jelly, paraffin, and stearic acid at a ratio of 55:43:2 by volume, for IM-20 and IM-21 the ratio was 45:45:10 and for IM-22 the ratio was 47:45:8. These parts were 10 cc rods formed in a steel die at 50 psi with the injection well at 71EC, the pipe at 71EC and orifice at 63EC. For these runs the mixer was turned off and the vacuum removed just prior to injecting each part. Each 10 cc bar was injected in 30 seconds and removed immediately after the pressure was completely released. The vacuum was then reapplied and the mixer turned on during the cooling of the mold. The part was then removed from the mold and the process repeated. The binders were removed in flowing Ar by packing the parts in sand in graphite boats and removing the binder according to a schedule derived from TGA experiments. Some of the rods from IM-19 were sintered without isopressing (No Iso), while bars from the same run were isopressed to 50 ksi, following binder removal. Sintering then took place at 1450EC in the batch LPHIP at ORNL and in the continuous furnace (belt speed 1.5"/min) at SIUC. These processes have been documented in previous reports.

These results show that isopressing improved the sintered density for both sintering methods. Also the batch sintering method produced the higher density of the two techniques. The hardness and microstructures are currently being determined.

<u>Status of Milestones</u>

1. Refine Economic Model and Design for Chosen Furnace Configuration — Completed
2. Continue Evaluation of Sintering Parameters on Properties of Selected Si_3N_4 Compositions — Completed
3. Continue Evaluation of Low Cost Si_3N_4 Powders — Completed
4. Design and Construct Prototype Belt Furnace — Completed
5. Continuous Sintering of Inter-Metallic Bonded Carbides — On Schedule

Communications/Visits/Travel
Aaron Woods to ORNL to complete SEM and hardness results for thesis.

Problems Encountered
None

Publications and Presentations
"Continuous Sintering of NiCr and NiCrFe-TiC Intermetallics," D. E. Wittmer, A. Woods, F. Goransson, T. Tiegs, and P. Menchhofer. Abstract submitted to 2001 International Conference on Powder Metallurgy and Particulate Materials, PMTec 2001, May 3-17, New Orleans, LA

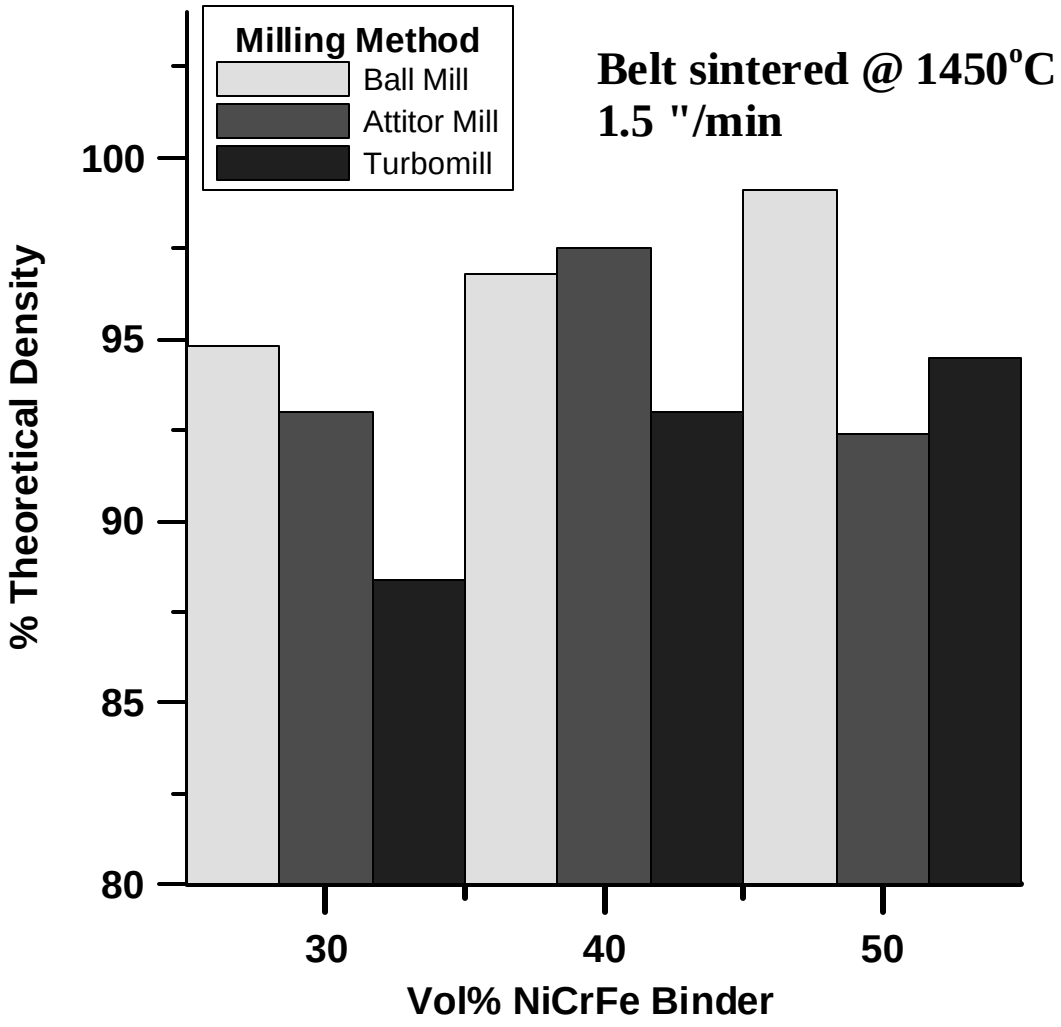

Figure 1. Density results for NiCrFe-TiC as a function of processing method, following continuous sintering at 1450EC at 1.5"/min.

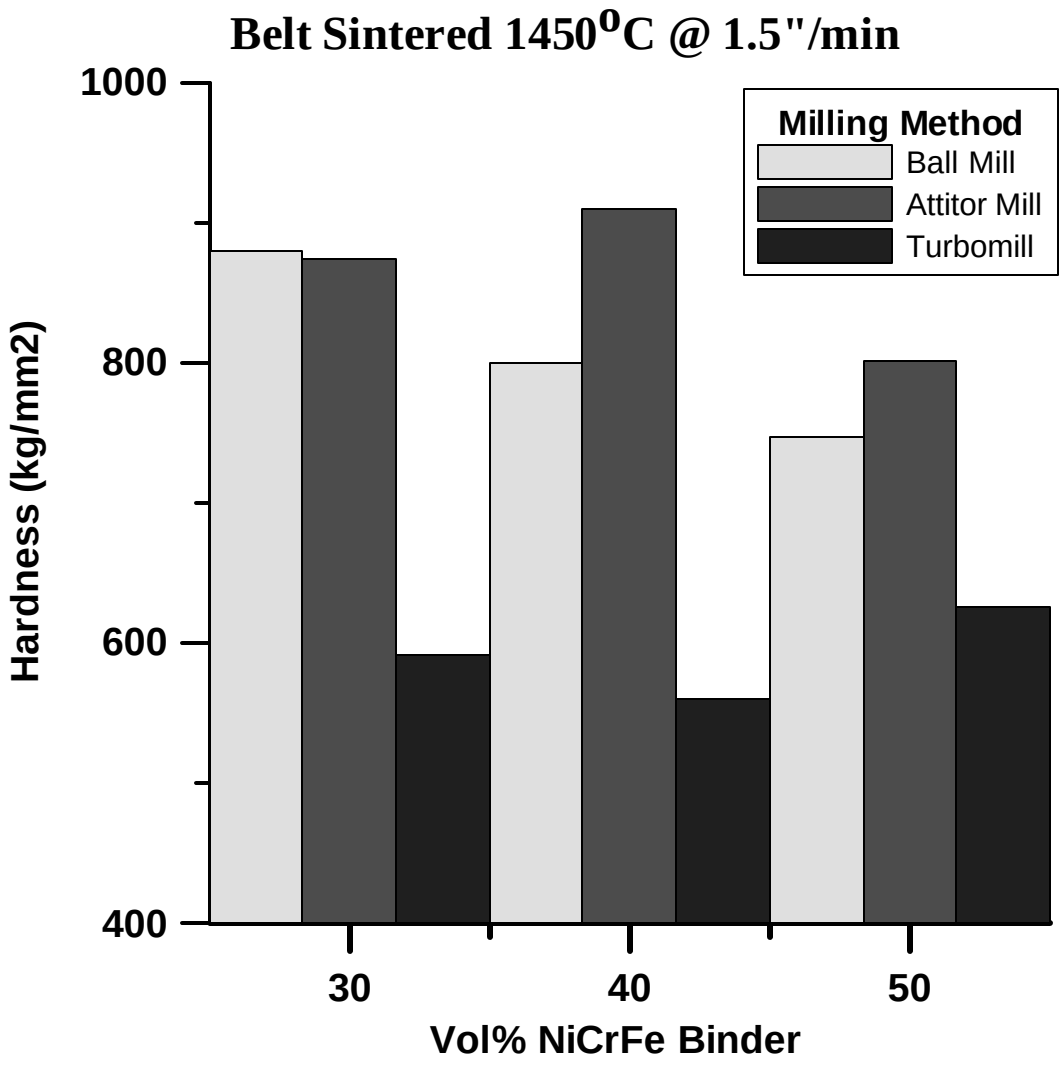

Figure 2. Hardness results for NiCrFe-TiC as a function of processing method and continuously sintered at 1450EC at 1.5"/min.

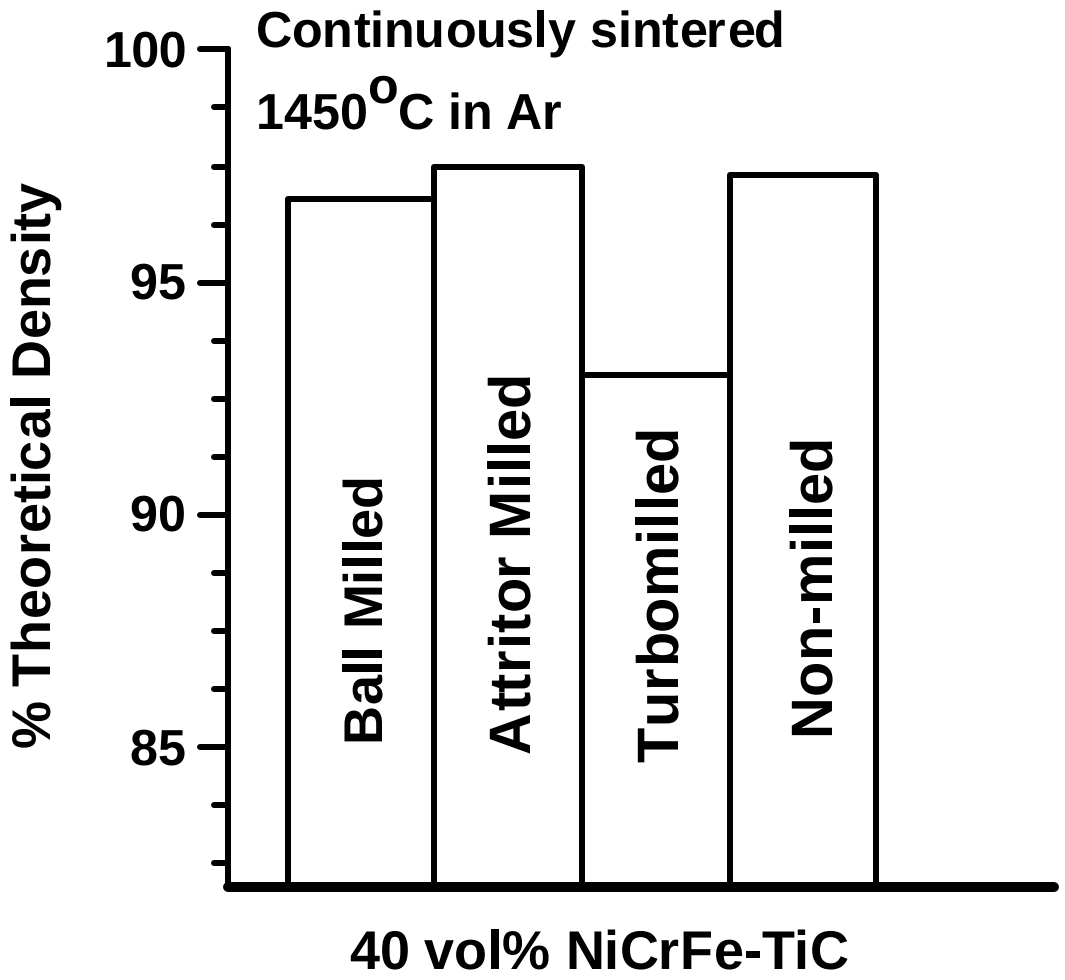

Figure 3. Density comparison for various processing methods that were continuously sintered at 1450E at 1.5"/min.

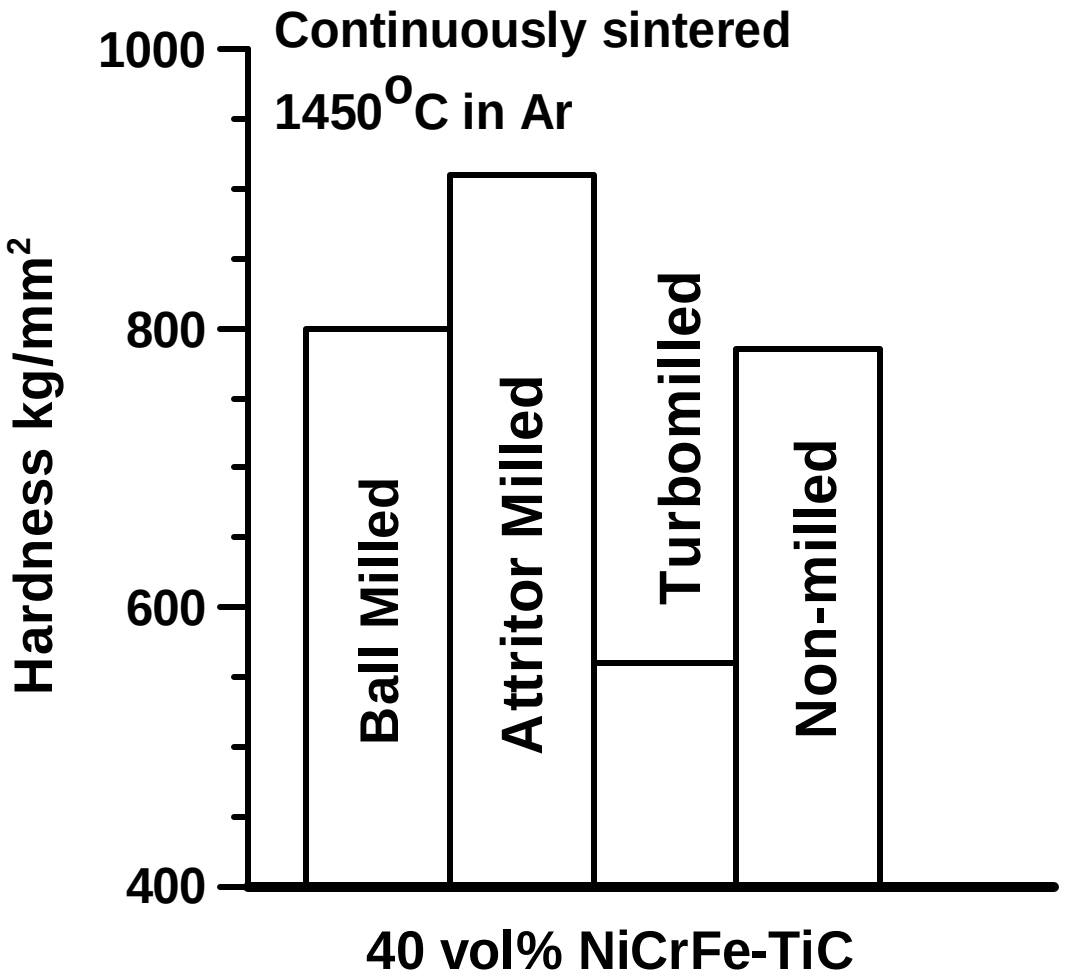

Figure 4. Hardness comparison for various processing methods following continuous sintering at 1450EC at 1.5"/min.

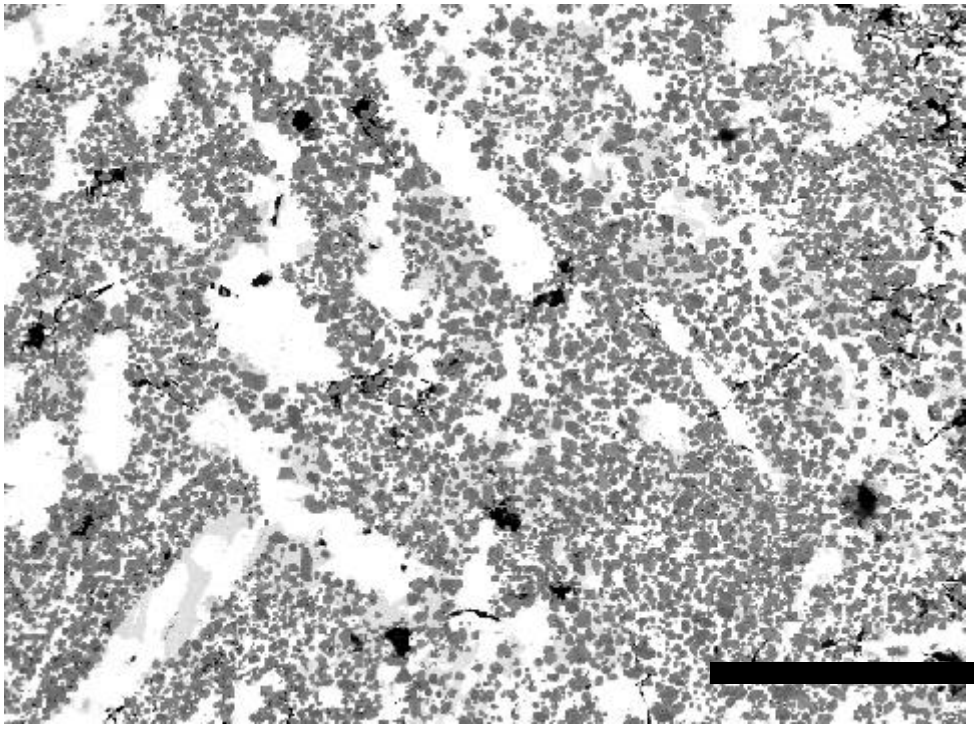

Figure 5. SEM photomicrograph of 40% NiCrFe-TiC composites processed by turbomilling and then continuously sintered Ar at 1450EC at 1.5"/min. (Bar = 50 Fm)

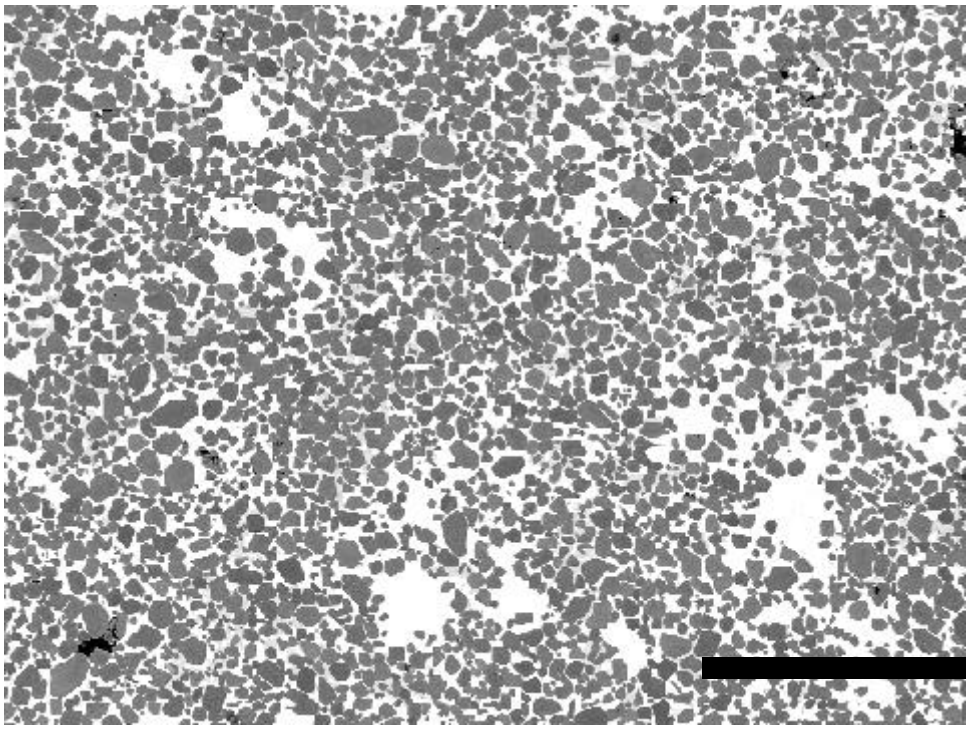

Figure 6. SEM photomicrograph of ball milled 40% NiCrFe-TiC continuously sintered in Ar at 1450EC at 1.5"/min. (Bar = 50Fm)

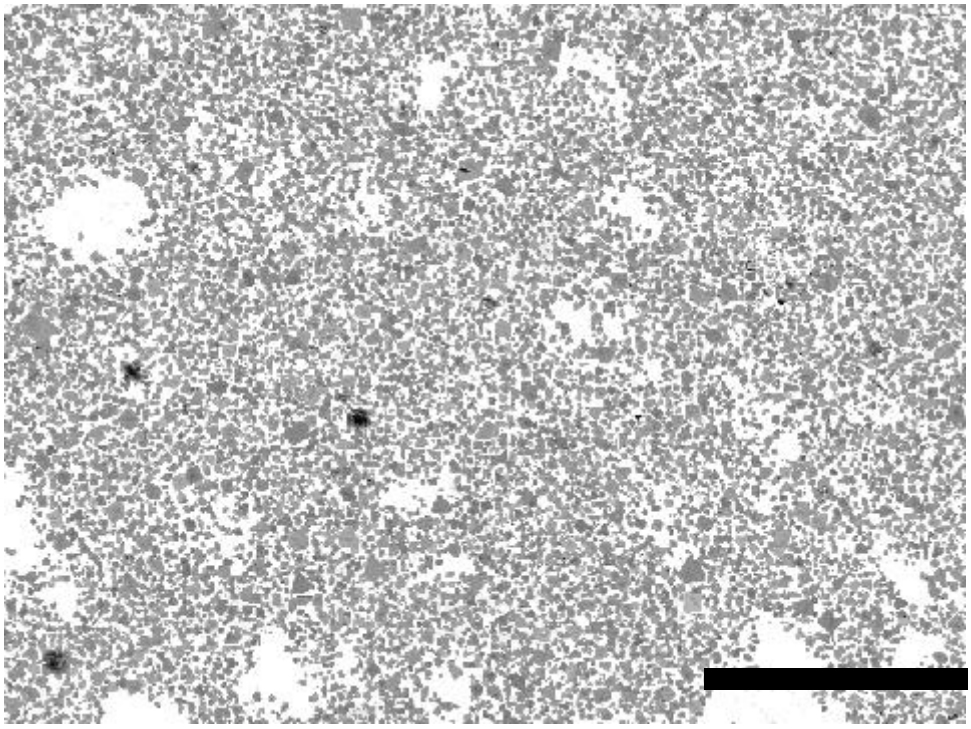

Figure 7. SEM micrograph of attritor milled 40% NiCrFe-TiC continuously sintered in Ar at 1450EC at 1.5"/min. (Bar = 50Fm)

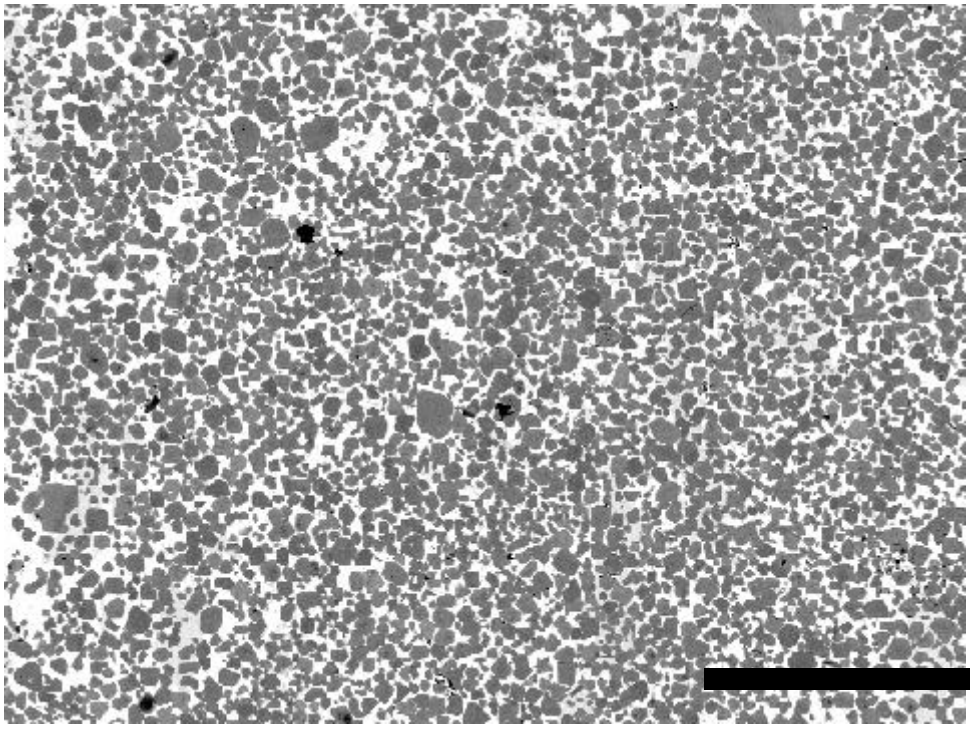

Figure 8. SEM photomicrograph of non-milled 40% NiCrFe-TiC continuously sintered in Ar at 1450EC at 1.5"/min. (Bar = 50Fm)

Low Cost-High Toughness Ceramics

T. N. Tiegs, F. C. Montgomery, P. A. Menchhofer, J. O. Kiggans, and D. L. Barker
Oak Ridge National Laboratory

Objective/Scope

Significant improvement in the reliability of structural ceramics for advanced diesel engine applications could be attained if the critical fracture toughness (K_{Ic}) were increased without strength degradation. Currently, the project is examining toughening of ceramics by two methods: microstructure development in oxide-based ceramics, and incorporation of ductile intermetallic phases.

Technical Highlights

Previous studies have shown that the properties of the aluminide-bonded ceramics (ABC) are attractive for diesel engine applications and consequently, development of these materials was started. At the present time, TiC-40 vol. % Ni_3Al composites are being developed because they have expansion characteristics very close to those for steel. Preliminary wear testing indicated that improved wear resistance could be achieved by decreasing the grain size of the TiC. Achieving fine grain size with the high binder contents is difficult because of the large inter-grain distances. In addition, it was thought that changing the TiC grain shape from a highly faceted one to a more rounded equiaxed grain would reduce localized stress at sharp corners. This, in turn, would improve abrasion resistance from any wear debris. Consequently, grain size refinement is presently being studied. Several approaches can be used to control the final TiC grain size. The methods studied in the present report include: (1) use of additives to change the interface behavior of the growing TiC grains, and (2) reduction of the initial TiC particle size.

Reduction of Oxygen Pickup During TiC Milling by Use of Additives

Previous work has shown significant oxygen pickup when the TiC was milled to particle sizes <0.5 µm. One of the methods to minimize oxygen pickup by non-oxide materials is to add surfactants that will absorb onto the 'fresh' surfaces and physically prevent oxygen from interacting with the surface. Several samples were fabricated (as indicated in Table 1), where oxalic acid or polyvinylpyrrolidone (PVP) were used to inhibit oxygen pickup. Another method, that is used in the hardmetals industry, is to mill the carbide powders with the metal particles and 'smear' the metal over the carbide surfaces. This method was also used as shown in Table 1.

TMPO-1 (30 and 60 minutes) is just the TiC where oxalic acid has been added to prevent oxidation during milling. Milling was done in a small (750 ml) attritor mill and appears to be not as effective as the large mill shown in previous experiments. It was run at 500 rpm (vs. 400 for large mill) to compensate for the lower tip speed. The TMPO-1-70 sample is after adding the Ni and NiAl powders and milling for an additional 10 minutes. TMPO-2 and -3 show the effect of adding the Ni and NiAl to the TiC from the beginning. As mentioned, the idea there was to prevent oxidation by smearing metal on the exposed TiC surfaces. Oxalic acid was also added in the TMPO-2 samples. TMPO-3 had oxalic acid plus PVP additions to absorb onto the TiC surfaces.

TMPO-1 samples give baseline data to compare to the other samples to see if oxidation can be decreased by additions that will absorb onto the surfaces. TMPO-2 shows a small effect of milling the Ni and NiAl along with the TiC to decrease oxygen pickup. However, TMPO-3 indicates PVP additions are very effective for preventing oxidation.

Microwave Sintering of TiC-Ni_3Al Composites

Prior research has indicated that microwave sintering of powder metals and cermets offers some advantages compared to conventional heating.[1-3] Consequently, several batches of TiC-40 vol. % Ni_3Al composites were pressed into discs and heated in a 2.45 GHz microwave cavity. The series of experiments are summarized in Table 3.

As shown, the initial attempt was to sinter the composites where the microwave energy coupled directly with the parts. Heating was adequate up to temperatures of 700-1000°C, however the runs were aborted after that because of poor heating even at relatively high power levels. Prior to heating, the approximate electrical conductivity of the pressed green parts was >2 O•cm due to limited particle-particle contact and some residual oxides on the surfaces of the TiC and metal particles. After heating to these intermediate temperatures, the approximate electrical conductivity of the non-densified parts was measured at <0.2 O•cm. Sintered dense samples exhibit conductivities <0.1 O•cm. While the prior research on the metal parts has shown the use of secondary coupling materials (often referred to as hybrid heating), recent claims have been made that no additional microwave absorbing material is necessary. The present tests indicate that once the powdered metal part develops sufficient electrical conductivity, the direct heating by microwaves is diminished.

The next step was to use alumina-30% zirconia (ZTA) as a coupling material, but this did not improve the heating ability of the samples in the microwave. By using zirconia fiber, which couples well at temperatures =700ºC, as a packing material, stable high temperatures could be achieved and densification was obtained. However, the heating of the samples was non-uniform at low temperatures and some cracking, which appeared to have occurred prior to densification was evident. Even the use of a BN spacer as a heat distributor (which had been successful with silicon nitride), did not alleviate non-uniform heating at low temperatures. On the other hand, B_4C grit couples well with microwaves even at room temperature and so was used as a packing material. In that case, heating uniformity was quite good and several samples were sintered to high densities at heating rates up to 20°C/min. The dense samples are currently being machined into mechanical test specimens and being polished for microstructure characterization.

Status of Milestones

On schedule.

Communications/Visits/Travel

None.

Problems Encountered

None.

Publications

T. N. Tiegs, J. Stephan, and K. McNerney, "Grain Refinement in TiC-Ni_3Al Composites," C/ORNL99-0557, (2001).

References

1. R. Roy, et al, "Full Sintering of Powdered Metal Bodies in a Microwave Field," Nature, Vol. 399, 668-670 (1999).

2. S. Gedevanishvili, et al, "Microwave Combustion Synthesis and Sintering of Intermetallics and Alloys," J. Mater. Sci. Lett., 18, 665-668 (1999).

3. D. Agrawal, "Metal Parts from Microwaves," Mater. World, 17 [11] 672-673 (1999).

Table 1. Summary of results on samples to minimize oxygen pickup for different TiC-40 vol. % Ni_3Al composites .

Sample No.	Oxalic Acid Addition (wt. %)*	PVP Addition (wt. %)*	Ni & NiAl Milled With TiC	Sintered Density (% T. D.)
TMPO-1	2	0	No	100
TMPO-2	2	0	Yes	99.8
TMPO-3	1	1	Yes	99.1

Table 2. Summary of results on particle size and oxygen content for different TiC-40 vol. % Ni_3Al composites .

Sample No.	Mean Particle Size (µm)	D_{90} Particle Size (µm)	Oxygen Content (wt. %)
TMPO-1-30	0.78±0.26	1.73	N.D.
TMPO-1-60	0.80±0.26	1.75	1.28
TMPO-1-70	1.93±0.73	5.5	0.74
TMPO-2-30	3.28±1.05	7.0	N.D.
TMPO-2-60	2.76±0.92	6.0	0.56
TMPO-3-30	4.12±1.38	9.5	N.D.
TMPO-3-60	0.87±0.29	2.0	0.22

Table 3. Summary of results on microwave sintering of TiC-Ni_3Al composites. Sintering was done under an argon-4% hydrogen atmosphere at 1400°C for 40 minutes.

Sample No.***	Insulation Type*	Spacer Type	Air Gap	Heating Rate (°C/min)**	Sintered Density (g/cm^3/% T.D.)	Comments
MW-1-1,2	None	BN	No	10/20	N.A.	Run aborted. Plasma at ~1000°C.
MW-2-1,2	ZTA	ZTA	No	10/20	N.A.	Run aborted. Temp. deviation >50°C at ~700°C.
MW-2-1a,2a†	ZrO_2 fiber	ZTA	No	10/20	99.6, 99.6	Sample 2a cracked.
MW-2A-1,2	ZrO_2 fiber	BN	Yes	10/20	99.2, 99.3	Sample 1 cracked.
MW-2-3,4	B_4C grit	BN	Yes	10/20	98.7 ,98.3	Samples looked good.
MW-2A-3,4	B_4C grit	BN	Yes	10/20	99.4, 99.2	Samples looked good.
MW-2-5,6	B_4C grit	BN	Yes	20/20	98.0, 96.8	Samples looked good.
MW-2A-5,6	B_4C grit	BN	Yes	20/20	99.7, 99.7	Samples looked good.

* ZTA - alumina/30 % zirconia; BN - boron nitride.
† Refire of the previous samples MW-2-1 and -2.
** Rate from room temperature to 1000°C/Rate from 1000 to 1400°C.
*** Two samples (~85 g each) were fired at the same time.

Intermetallic-Bonded Cermets

P. F. Becher, C. G. Westmoreland, and S. B. Waters
Oak Ridge National Laboratory

Objective /Scope:

The goal of this task is to develop materials for diesel engine applications, specifically for fuel delivery systems and wear components (e.g., valve seats and turbocharger components). This will require materials which have a minimum hardness of 11 GPa and a thermal expansion coefficient of 10 to 15 x 10^{-6}/°C over the temperature range of 25° to 300°C. The material should also have excellent corrosion resistance in a diesel engine environment, flexure strength in excess of 700 MPa, and fracture toughness greater than 10 MPavm to ensure long-term reliability. The material should also be compatible with steels and not cause excessive wear of the steel counter face. The upper temperature limit for fuel delivery systems applications is 540°C, and for the other wear applications, the limit is 815°C. Finally, the total material processing costs for these advanced materials should be competitive with competing technologies such as TiN or other ceramic coatings on high-speed tool steels.

Technical Highlights:

Attritor milling of commercial TiC powders has been successfully utilized to fabricate fully dense TiC-Ni_3Al cermets with submicron TiC grain sizes by pressureless sintering. However based on current experience, various parameters must be controlled. The use of finer WC milling media was most efficient in reducing the TiC particle size while minimizing the increase in the oxygen content of the TiC powder after milling and drying the powder, Table I. The finer zirconia media was much less efficient in reducing the TiC powder size and required longer milling times, which led to significant increases in the final oxygen content of the TiC powder. When the oxygen content of any submicron TiC powder exceeded 2 to 2.5 wt. %, sintering the cermets to full density was not possible. Finally, sintering under a mild vacuum has proven to be the most successful route for achieving fully dense submicron TiC grain size cermets combined with high flexure strengths. As noted in Table I, these characteristics are obtained only when a vacuum less than 100 microns is maintained during the elevated temperature portion of the sintering cycle.

Status of Milestones:

On Schedule

Communication/Visits/Travel

Discussions held with Jim Stephan of AMT/CoorsTek on our analysis of reaction sintered TiC-40 vol. % Ni_3Al cermets supplied by him.

Publications

K.P. Plucknett and P.F. Becher, "TiC/Ni_3Al Composites Prepared by Melt-infiltration Sintering: Processing and Microstructure Development," *J. Am. Ceram. Soc.*, in press.

References

None

Table I. Processing parameters for TiC-40 vol. % Ni_3Al Cermets

Weight Ratio of TiC:Media[*]	Media	Milling Time, h	Particle Size,[b] µm D90/D50	Weight % Oxygen[c]	Sintering Conditions, °C/h/vacuum[d]	Binder Phase[e]	Density % T.D.[f]	Fracture Strength, MPa
TiC K767	NA 2 mm ZrO_2	NA =12	/2.6 /0.5	0.7 3.9	1350/1/<100 1500/1/<100		= 90 90	N.D. N.D.
TiC K-02000 K-01000	N/A N/A	N/A N/A	5.2/2.8 3.9/1.2	0.5 0.8				
10:1	1.1 mm WC	6	0.89/0.44	1.4	1300/1/<100 1450/1/<100	Ni_3Al	100 100	1032±134
10:1	1.1 mm WC	6	0.89/0.44	1.4	1250/1/<100 1400/1/<100	(NiAl + 2 Ni)	100 100	1190±149
10:1	1.1 mm WC	6	0.89/0.44	1.4	1430/1/500	(NiAl + 2 Ni)	98	704 ± 83

a. 750 ml Attritor Mill (TiC fraction includes 2 wt. % Mo and isopropanol used as liquid phase).
b. D90 – 90 % by weight with size = that shown; D 50 – 50 % by weight with size = that shown.
c. Combustion analysis, LECO.
d. Vacuum level in microns.
e. Binder phases added either as or as a mixture of (NiAl+2Ni---reaction sintering).
f. T. D. – theoretical density.

Low-Cost Manufacturing of Precision Diesel Engine Components

S.B. McSpadden, Jr.
Oak Ridge National Laboratory

Objective/Scope

To develop and demonstrate optimized, cost-effective grinding processes for the production of ceramic components for use in diesel engines. To develop and demonstrate optimized, cost-effective, non-destructive testing methods for the detection and prevention of machining-induced damage in ceramic components.

Technical Highlights

Caterpillar CRADA – Experimental activities for this CRADA are complete and reports have been received from the principal investigators for all ORNL sub-tasks. A compilation of results from the individual tasks is nearing completion and will be sent to Mr. Jeff Thiele at Caterpillar for review.

Cummins CRADA – At Cummins Engine Company's request, the remaining effort for the existing CRADA will be applied to on-machine temperature measurement studies at the grinding interface.

State Partnership Program Proposal Submitted for the Investigation of Non-Destructive Detection of Flaws in Ceramic Diesel Engine Fuel System Components – The subject proposal was prepared jointly by ORNL, Cummins Engine, CoorsTek, and the Indiana and Colorado state energy offices and submitted for internal review at ORNL. The proposal requested $50K of ORNL (DOE) funding with in-kind contributions from the other participants. The objective of the project is to investigate non-destructive measurement techniques that are capable of detecting sub-surface machining damage in ceramic components. This is an area of great interest to Cummins. Although some laboratory techniques show promising results, the challenge is to find a relatively inexpensive, robust method that can be used in a production environment. Scanning acoustic microscopy, resonant ultrasound, x-ray and laser-based techniques are among those being considered. Should this proposal be approved, we intend to augment the project with available funds from OHVT. This work is well within the stated objective/scope of the *Cost-Effective Machining of Ceramic Engine Components* task and is included as a part of our 2001 Annual Operating Plan.

Collaborations with North Carolina State University Continuing – Dr. Albert Shih, Associate Professor of the N.C. State University Materials Science and Engineering Department, is currently involved with numerous collaborative efforts with the HTML Machining and Inspection Research Group, most of which are relevant to the cost-effective machining of ceramic engine components. Three of his students will be working at the HTML in late January, 2001, investigating the performance of grinding wheels used to grind ceramic components under various operating conditions. The current phase of work on the measurement of temperature at the grinding wheel/workpiece interface, being performed by Mr. Adam Curry, is nearing completion.

Communications/Visits/Travel

A trip to Caterpillar's Peoria facility is planned for late February. We will discuss short-term and strategic areas of mutual interest that should be supported by the HTML Machining and Inspection Research Group. This information will be used to better focus the group's ceramic machining/inspection/tribology activities.

Our plans to procure a state-of-the-art surface grinder (through a 4-year lease) are proceeding. This is a critical need for the Machining and Inspection Research Group. Two competing brands of grinders with roughly equivalent capabilities are currently being evaluated. The present-value cost of the grinder is approximately $160,000, which translates into $200,000 after all taxes, overhead, and installation costs are added. Although we do not have sufficient capital or operating funds to make an outright purchase at this time, the leasing option appears to be viable. However, DOE approval will be required, and has been requested.

Publications

Krueger, M. K., S. C. Yoon, D. Gong, S. B. McSpadden Jr.,* L. J. O'Rourke,* and R. J. Parten,* "New Technology in Metalworking Fluids & Grinding Wheels – Achieve 130-Fold Improvement in Grinding Performance," *Abrasives Magazine*, 8-15 (October/November 2000).

Cylindrical Wire Electrical Discharge Machining (EDM) and Temperature Measurement

Albert Shih
North Carolina State University

Objective/Scope

To develop precise, efficient, and cost-effective cylindrical Wire Electrical Discharge Machining (WEDM) process for cermet and other electrically conductive advanced engineering materials and temperature measurement methods for grinding and diesel exhaust aftertreatment devices.

Technical Highlights

Three highlights in this quarter are the design and manufacture of the prevision underwater spindle, experiments to find the maximum material removal rate, and the surface finish measurement of cylindrical wire EDM parts.

1. Spindle Design:

The spindle has to meet four design requirements: accuracy, flexibility, electrical connection for high current flow, and corrosion resistance. Pictures and schematic drawing of the new underwater spindle used in the study are shown in Figs. 1 and 2, respectively. A pair of deep groove silicon nitride ball bearings with stainless rings, made by Barden, was used. The gear motor is located above water on the top of the stand. A timing belt is used to transmit the rotational motion to the R8 collet holder. Precision internal grinding of the angle in collect holder is required to achieve the desired less than 5 μm runout specification on the part. Two back-wired electrical carbon brush was used on the front of the spindle. The contact surface between the carbon brush and the shaft is gradually oxidized and needs to be clean periodically to avoid burning brush's back wire due to high electrical current flow. After several failed spindle design, we finally have a good, precise spindle for the cylindrical wire EDM development. The assistance from the Experimental Machining Lab at Cummins Technical Center in the design, manufacturing, and assembly of this spindle is greatly appreciated.

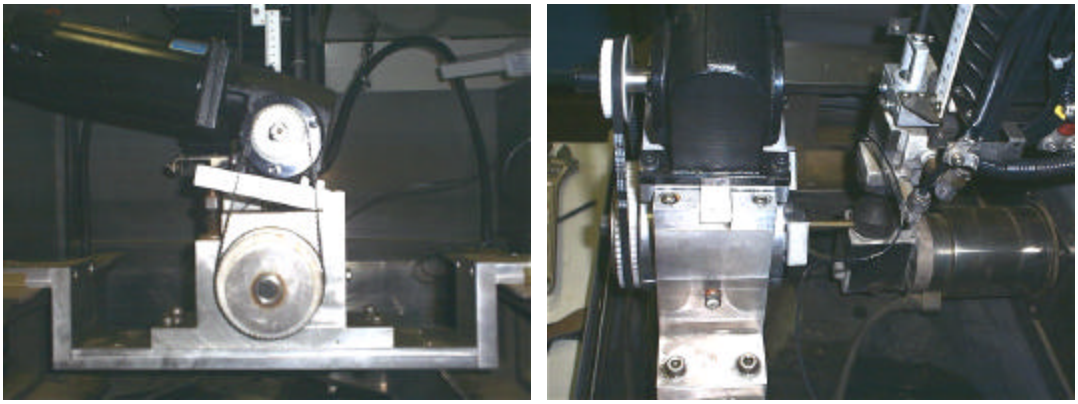

(a) Front View (b) Side View

Fig. 1. Front view and side view of the hybrid bearing underwater spindle.

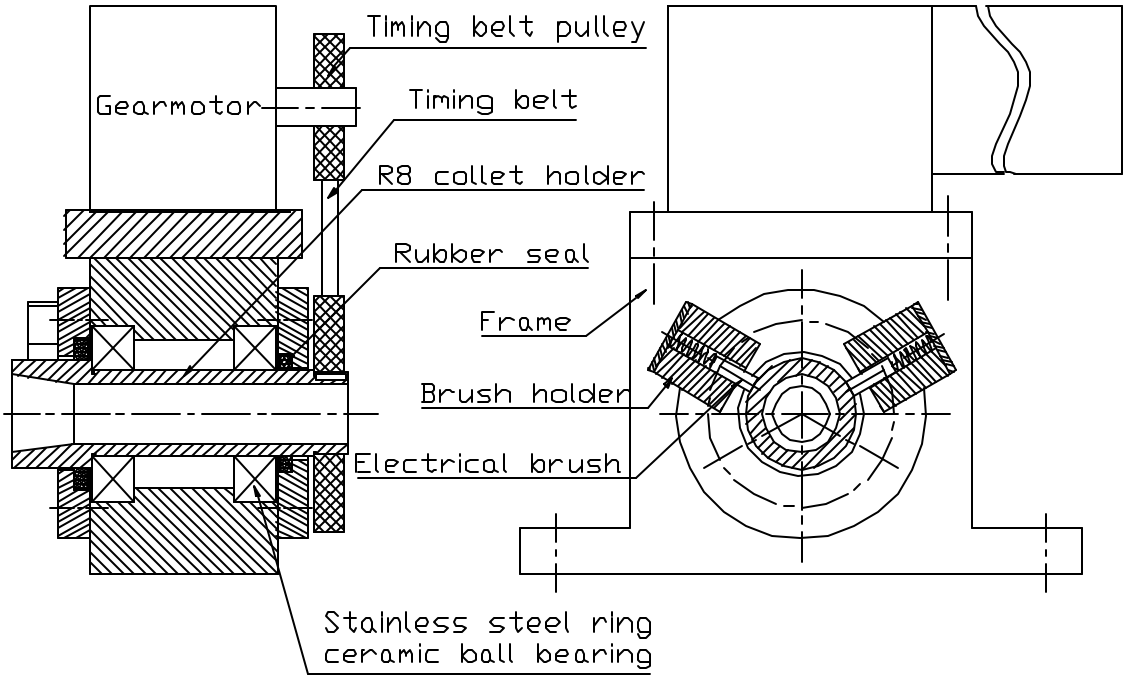

Fig. 2. Schematic of the underwater spindle for cylindrical wire EDM.

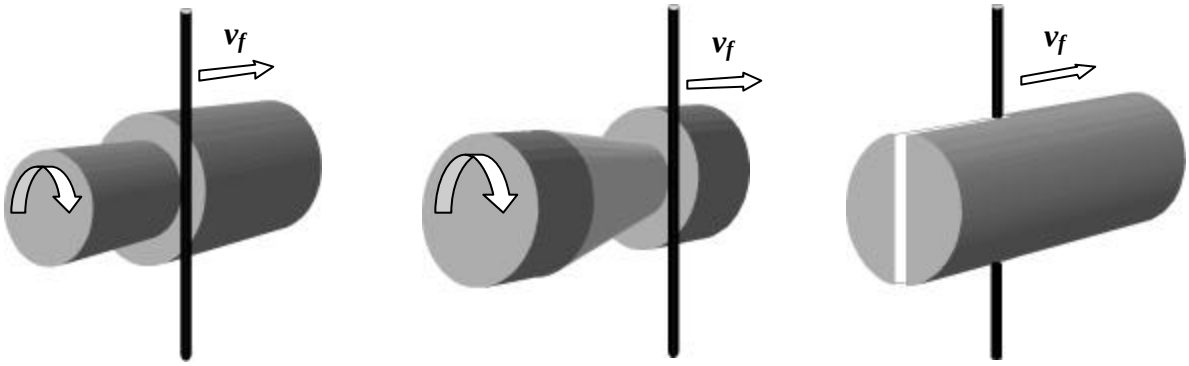

(a) (b) (c)

Fig. 3. Experiment configuration to find the maximum material removal rate, (a) a=0 and gradually increasing v_f, (b) constant α and v_f, and (c) 2D wire EDM. (Note: a is the angle between the wire traverse velocity vector and the rotating axis)

2. Maximum Material Removal Rate (MRR_{max}):

The three test configurations to find the maximum material removal rates in cylindrical and 2D wire EDM are illustrated in Fig. 3. In Fig. 3(a), the angle between the wire traverse velocity vector, $\boldsymbol{v_f}$, and the rotating axis, denoted as a, is set to 0 degree. The traverse speed of the wire across the part, v_f, is gradually increasing to the limit until the continuous wire breakage occurs. Another test configuration to find the maximum material removal rates in cylindrical wire EDM with constant a and v_f is shown in Fig. 3(b). The material removal rate is gradually increasing. At the limit when the short circuit error occurs, the material removal rate is recorded as MRR_{max}.

Figure 3(c) shows the test configuration to determine the maximum material removal rate for 2D wire EDM. Experimental results for the carbide and brass work-materials using the three test configurations shown in Fig. 3 are summarized in Tables 1 to 3. In Table 1, R is the radius of the original rod, r is small radius of the workpiece after cutting, and $v_{f,max}$ is the maximum wire traverse speed during cutting. In Table 2, r_{min} is the minimum possible diameter of the shaft achievable during cutting. In Table 3, t is the thickness of the groove cut by 2D wire EDM.

Table 1. MRR_{max} for the cylindrical wire EDM test configuration shown in Fig. 3(a) (a=0 and gradually increasing v_f)

Material	R (mm)	3.18			2.54	
	r (mm)	2.54	1.59	0.75	1.59	0.75
Brass	$v_{f,max}$ (mm/min)	5.72	2.69	2.13	5.33	3.46
	MRR_{max} (mm^3/min)	**65.2**	**64.1**	**63.7**	**65.7**	**64.0**
Carbide	$v_{f,max}$ (mm/min)	1.42	0.81	0.66	1.55	1.02
	MRR_{max} (mm^3/min)	**16.2**	**19.3**	**19.7**	**19.1**	**18.9**

Table 2. MRR_{max} for the cylindrical wire EDM test configuration shown in Fig. 3(b) (constant a and v_f)

Material	a (degree)	-15	-30	-45
Brass	r_{min} (mm)	2.16	2.01	1.65
	MRR_{max} (mm^3/min)	**65.5**	**68.3**	**69.6**
Carbide	r_{min} (mm)	2.02	1.95	1.17
	MRR_{max} (mm^3/min)	**19.1**	**18.7**	**20.9**

Table 3. MRR_{max} for the 2D wire EDM test configuration shown in Fig. 3(c)

Material	t (mm)	r_e (mm)	$v_{f,max}$ (mm/min)	**MRR_{max} (mm^3/min)**
Brass	6.35	0.183	23.9	**55.5**
Carbide	6.35	0.163	4.32	**8.90**

Several observations can be extracted by comparing the data in Tables 1 to 3.

(a) The brass has much higher material removal rate than the carbide.
(b) The results from the two test configurations for cylindrical wire EDM at different sizes and angles are consistent. This also verifies the mathematical model for the cylindrical wire EDM MRR presented in the previous report [Qu et al., 2000].
(c) The MRR_{max} for cylindrical wire EDM is greater than 2D wire EDM, possibly due to better flushing condition during the cylindrical wire EDM.
(d) At steeper angle a, wire breakage is more likely to occur during cutting.

3. Surface Finish

A set of parts was produced to investigate the effect of part rotational speed, w, and wire traverse speed, v_f, on the part roundness and surface finish. Twelve experiments at three different v_f and four different w were conducted on each of the work-material, brass and carbide. The experiment and analytical results are shown in Fig. 4.

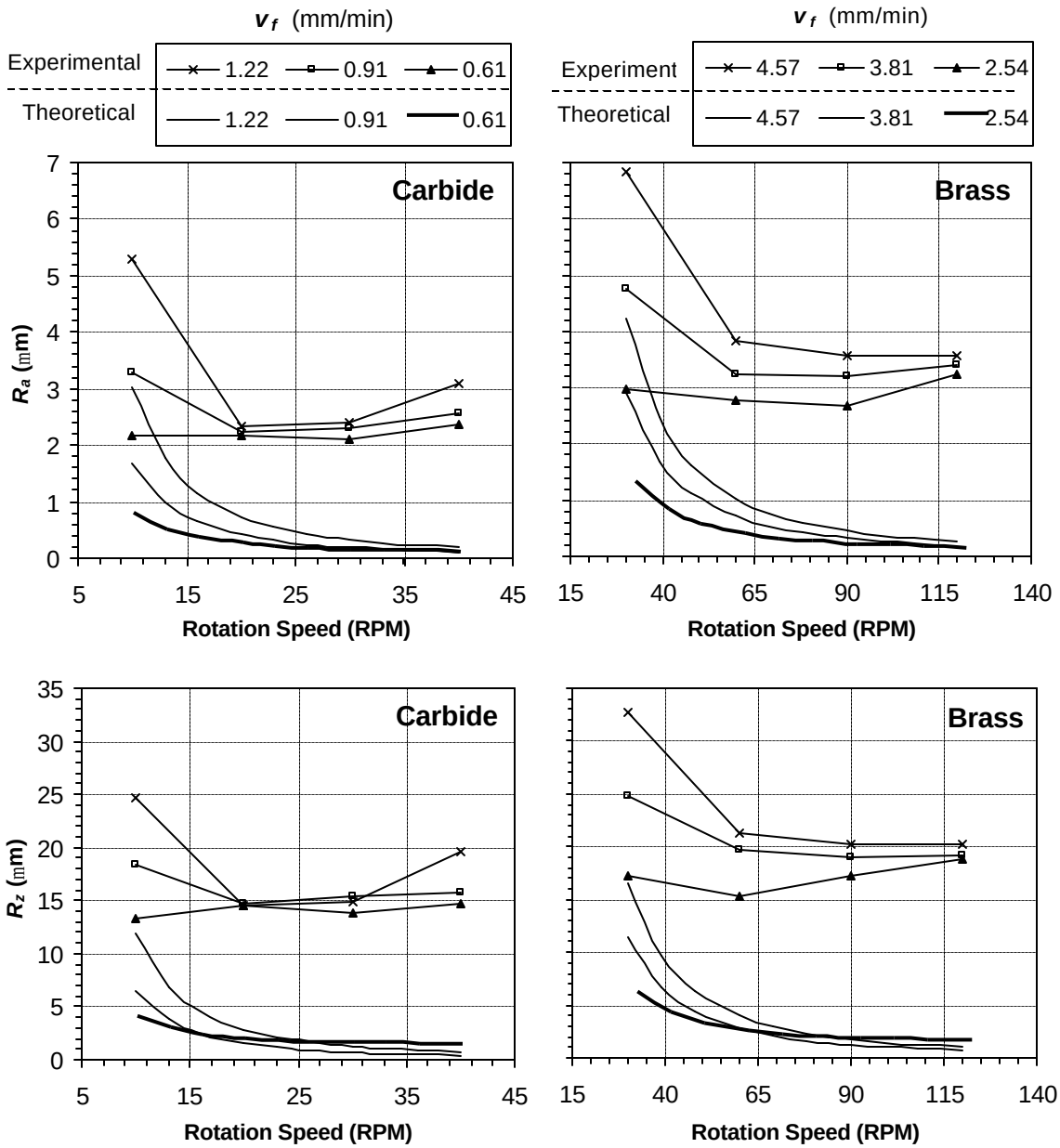

Fig. 4. The surface finish of cylindrical wire EDM parts.

Several observations can be extracted from Fig. 4.

(a) Better surface finish can be seen at higher w and lower v_f.
(b) The analytical results from modeling under estimate both the R_a and R_z. The modeling does not include the surface finish generated by the EDM itself. The gap between the analytical and experimental results is about 2 μm R_a and 3 μm R_z for the brass and 3 μm R_a and 4 μm R_z for the carbide.
(c) The surface finish is, in general, rough on the cylindrical wire EDMed surface.

Status of Milestones

Milestone 1: Develop process technology to achieve high material removal rate in cylindrical WEDM of advanced engineering materials.
Status: Experiments were conducted to quantify the maximum material removal rate. Results showed the maximum material removal rate in cylindrical wire EDM is higher than the conventional 2D wire EDM.

Milestone 2: Determine the level of form tolerances and surface finish achievable by the cylindrical WEDM.
Status: Experiments was conducted at High Temperature Materials Lab at Oak Ridge National Lab to measure the roundness and surface finish (using both contact and non-contact methods) of cylindrical wire EDMed brass and carbide parts.

Milestone 3: Prototype needles, armature pins, and plungers for diesel engine fuel injectors.
Status: Exploratory experiments to machine miniature shafts in the size under 0.1 mm diameter were conducted. Chemical etching methods to remove the recast layer on brass and carbide parts were also tested.

Milestone 4: Develop mathematical models for material removal rate and surface finish of the cylindrical WEDM.
Status: Noting to report. The mathematical models for material removal rate and surface finish have been derived. These results have been summarized in a technical paper.

Milestone 5: Characteristics of the recast layer after WEDM and cylindrical WEDM and the surface condition after abrasive blasting.
Status: Experiments was conducted at High Temperature Materials Lab at Oak Ridge National Lab to use the SEM to observe the surface and cross-section of cylindrical wire EDMed brass and carbide parts.

Milestone 6: Development of optical fiber based temperature measurement method, with applications for grinding process and diesel exhaust aftertreatment filters.
Status: Grinding temperature measurement methods using the high-speed two infrared sensor method and the spectrometer were experimented. The concept and results were presented in the 2001 NSF Design, Service and Manufacturing Grantees and Research Conference.

Communications/Visit/Travel

Adam Curry, Jun Qu, and Albert Shih visited Cummins Engine Company and Oak Ridge National Laboratory in November 2000 to report the progress on infrared-based grinding temperature measurement and the cylindrical wire EDM process development. At Cummins, the machining and assembly of the underwater spindle were discussed.

Adam Curry and Albert Shih attended the 2001 NSF Design, Service and Manufacturing Grantees and Research Conference to present the concept of through-the-workpiece infrared temperature measurement method.

Publications

A technical paper entitled "Development of the Cylindrical Wire Electrical Discharging Process" by J. Qu, A. J. Shih, and R. O. Scattergood was submitted to the Symposium on Nontraditional Manufacturing Research and Applications in 2001 American Society of Mechanical Engineers International Mechanical Engineering Congress and Exposition.

References

J. Qu, A. J. Shih, and R. O. Scattergood, *Cylindrical Wire Electrical Discharge Machining Process*, Final Report for the Heavy Vehicle Propulsion System Materials Program, Office of Transportation Technologies, US Department of Energy, November 2000.

NDE Technology for Fuel Delivery and Insulating Materials

W. A. Ellingson
Argonne National Laboratory

Objective/Scope

The objective of the work in this task, part of the Testing and Characterization research area of the Heavy Vehicle Propulsion System Materials Program, is to develop enabling nondestructive evaluation/characterization (NDE/C) technology for lower cost and high performance materials. Specifically, this project addresses development of advanced NDE/C technology for a)-advanced fuel delivery systems (including injector nozzles) and b)-insulating materials for reducing heat losses in the combustion zone. Fuel delivery systems for heavy-duty diesel engines are complex, very expensive and represent a significant portion of the cost of a heavy vehicle diesel engine. High pressures inside these fuel delivery systems contribute to poor fuel delivery and hence poor emissions. Materials development is part of Goal 3 of the heavy vehicle propulsion materials program. Insulating materials are also a significant materials development area because of the improvement in engine efficiency if reduced heat losses can be obtained. NDE/C technology that can provide information for reliable cost production, quality assurance and engine component surveillance would be of benefit to reaching the goals.

Technical Highlights

NDE/C technology development continues to focus on fuel delivery and insulating materials with an emphasis on high performance ceramic materials.

Fuel Delivery Systems

We have been discussing the NDE effort on ceramic fuel metering plungers being conducted in cooperation with Cummins Engine Co. Figure 1 below shows a cross section of the Cummins Engine CELECT fuel injector system showing the location of the fuel metering plunger.

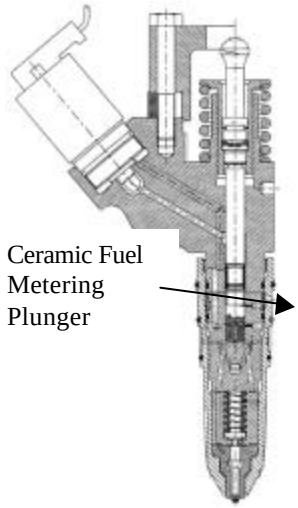

Figure 1
Schematic diagram of Cummins Engine fuel injector showing location of metering plunger

The efforts we have been undertaking have been to establish if the elastic optical scattering method could detect machining damage in these plungers. Figure 2 shows the locations on the plungers which have been of interest as well as the scan data from the entire surface. We have been studying three materials of interest. These are ceria-stabilized zirconia and magnesia-stabilized zirconia materials from two different companies.

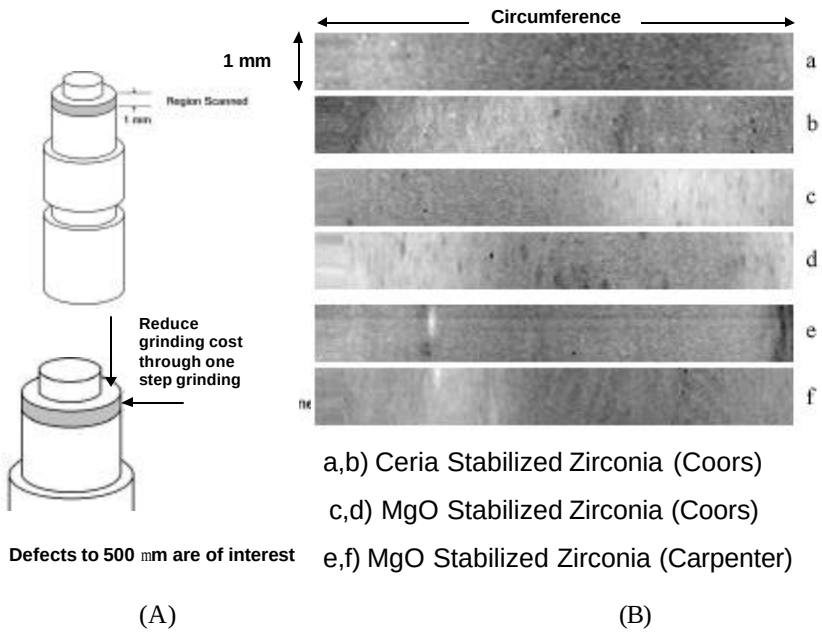

Figure 2
Schematic diagrams and laser scatter data from plungers
A)-schematic showing scanning location
B)-resulting data from the scans
Note that there were 2 samples of each material

By enlarging the scanned regions, correlations can be seen between the laser scan data and surface optical photomicrographs. That is, surfaces with more open pores correspond to laser data with more "black" spots indicating damage. This can be seen in Figures 3 through 5. Note that the initial scan data displayed were the "sum" image data. However, since we also obtain data from the ratio of the output of the two detectors, we also study the ratio images. In Figures 3 through 5 below, we used the ratio images to correlate to the surface optical photomicrographs.

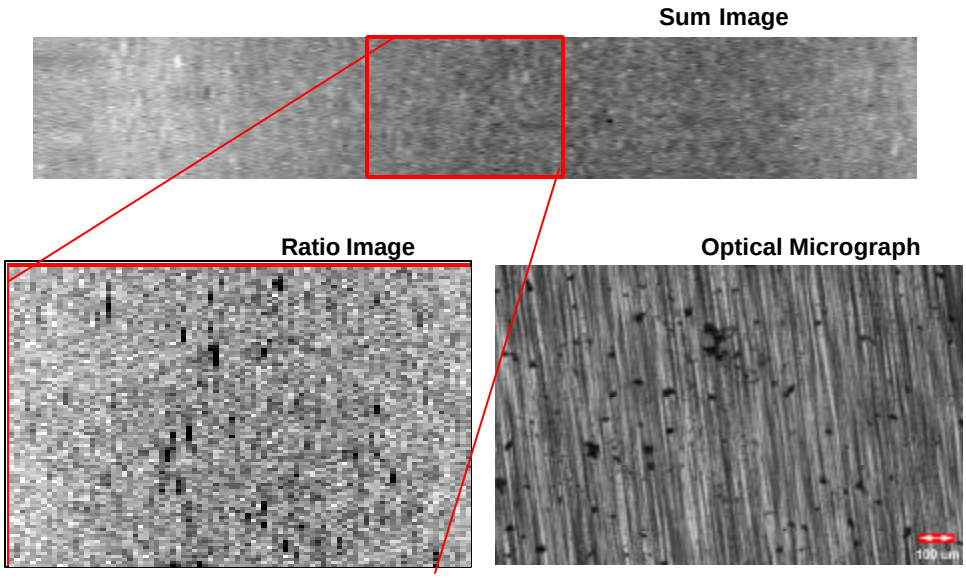

Figure 3
Correlation between laser scan image data and surface optical photomicrograph for ceria-stabilized zirconia

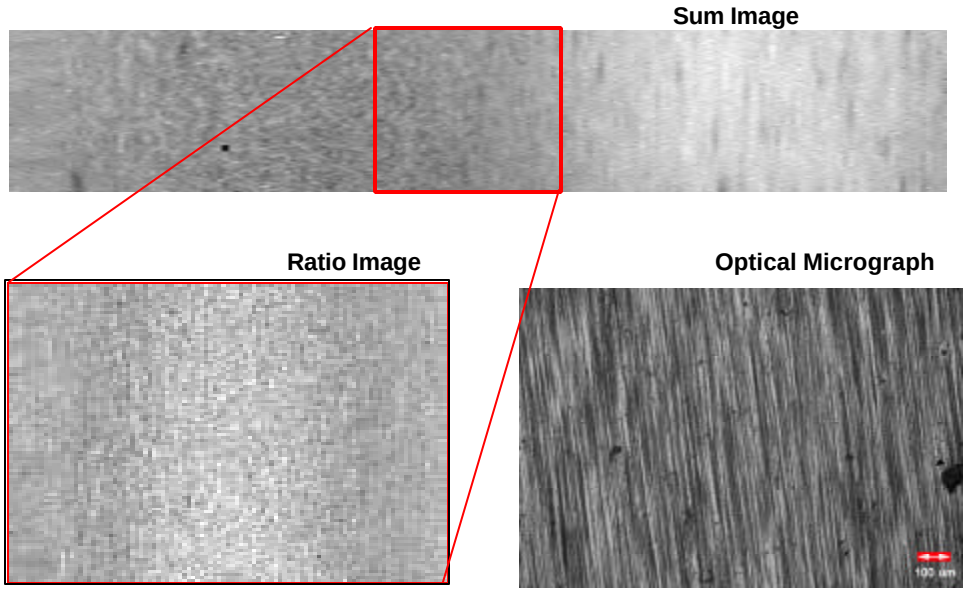

Figure 4
Correlation between laser scan image data and surface optical photomicrograph for magnesia-stabilized zirconia

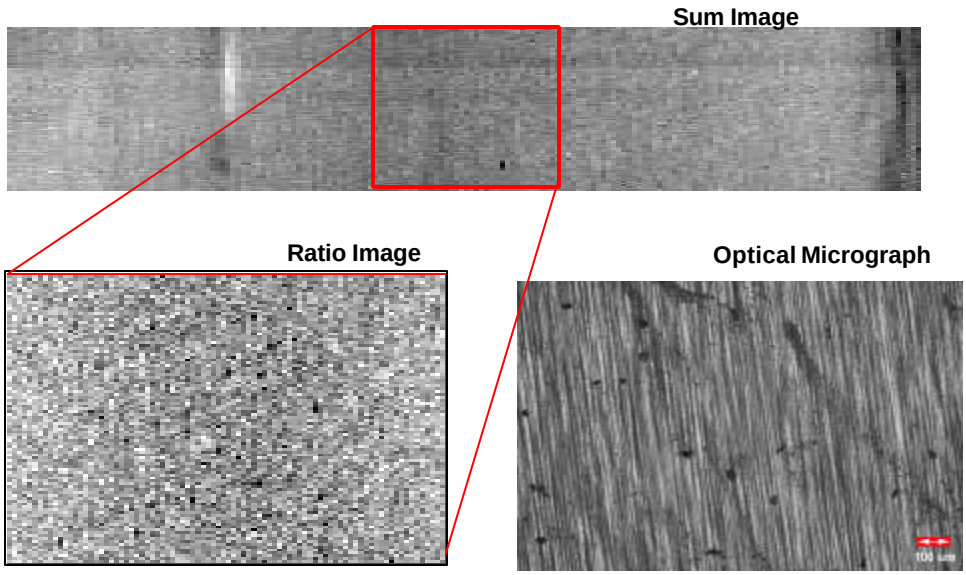

Figure 5
Correlation between laser scan image data and surface optical photomicrograph for magnesia-stabilized zirconia

By comparing the laser scan data to the optical photomicrographs, one can see that the relative number of open surface pores in the optical photomicrographs correspond to the "black" spots in the laser scan image data. We shall be analyzing these data in a more quantitative sense in the future.

NDE for Insulating Materials
We continue work on developing this aspect of this effort.

Communications/Visits/Travel
None

NDE Development for Ceramic Valves for Diesel Engines

J. G. Sun, A. Lindgren, W. A. Ellingson,
Argonne National Laboratory

and S. K. Lee
Caterpillar, Inc.

Objective/Scope

Emission reduction in diesel engines designated to burn fuels from several sources has lead to the need to assess ceramic valves to reduce corrosion and emission. The objective of this work is to evaluate several nondestructive evaluation (NDE) methods to detect defect/damage in structural ceramics valves for diesel engines. There are four tasks to be carried out in this work: (1) Establish correlation of NDE data with mechanical properties for fatigue/wear damaged samples. These include rotary fatigue, dynamic fatigue, impact/sliding wear, and possible thermal shock testing. The induced damage will be assessed using various NDE methods including dye penetrant, optical scatter, impact acoustic resonance (IAR), X-ray CT, thermal imaging, and others. NDE data will be correlated with those from characterization tests including mechanical strength, SEM, and others. (2) Develop NDE techniques for ceramic-metal joints. Effort will be focused on developing new methods as well as evaluating existing NDE techniques to characterize quality of ceramic-metal joints. NDE data will be correlated with mechanical data. (3) Conduct NDE studies of full-size engine valves. In this part of the work, full sized ceramic valves will be produced for testing in a single cylinder test engine. These valves will be examined using NDE techniques developed at Argonne. (4) Finalize correlation of NDE to machining damage. This limited effort will conclude the earlier work to correlate NDE data with mechanical properties of machining-damaged Si_3N_4 ceramics. Elastic optical scatter method will be used to examine these specimens and the NDE data will be correlated with flexural strength.

Technical Highlights

Work during this period (October-December 2000) focused on setting up NDE systems for detection interface cracks in ceramic-metal joints.

1. Elastic Optical Scattering NDE for Machining Damage

We continued developing and programming filtering schemes for calculation of statistical parameters from laser scatter data.

2. NDE Development on Joints

We are setting up the thermal imaging NDE system for evaluation of the steel-ceramic joints from Caterpillar, Inc. We have also conducted a sensitivity study to numerically simulate 1-D transient heat transfer in a 3-mm-long steel with an air-gap of 0.5-µm thickness at the middle of the steel. This air-gap thickness is about the same as the crack-gap thickness in the joint observed from the SEM data shown as Figure 2 in the August-September Bimonthly Report. The numerical result indicates that the thermal conductivity (or diffusivity) will be reduced by ~30% with the introduction of the crack (or air-gap) in the steel. Figure 1 shows a temperature profile in the steel, in which an instantaneous heat source was

applied at the left end. The temperature discontinuity at the crack location is apparent. Therefore, it is expected that thermal imaging NDE technique is capable of detecting cracks in the joint.

In preparation for ultrasonic scans of the joint, we have ordered and received 2 pairs of transducers with centering frequencies at 10MHz and 15MHz. High frequency transducers will allow us to detect small-sized cracks or defects. Mounting blocks to support and center the joints on a turntable were also machined. Work to scan the joints will start in the next period.

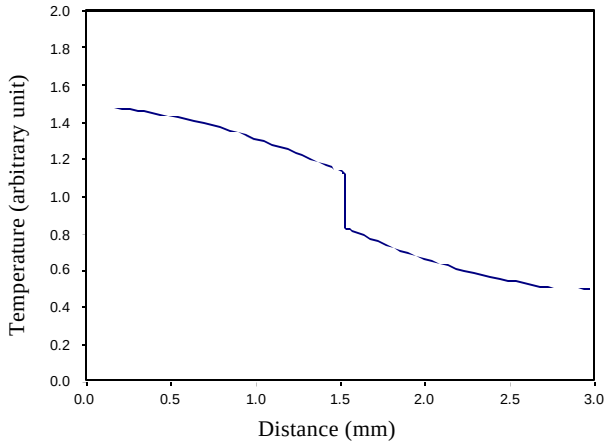

Figure 1. Temperature profile in a 3-mm steel with a 0.5-µm air gap at the middle.

Status of Milestones

Current ANL milestones are on or ahead of schedule.

Communications/Visits/Travel

J. G. Sun attended the ASM Materials Solutions Conf. & Expo.-2000 to be held Oct. 9-12, 2000 at St. Louis, MO and presented a paper on laser scatter study of machined ceramics for diesel engines.

W. A. Ellingson and J. G. Sun will attend the American Ceramic Society's 25th Annual International Conf. on Advanced Ceramics & Composites, Cocoa Beach, FL, Jan. 21-26, 2001.

Problems Encountered

None this period.

Publications

None this period.

Processing and Characterization of Structural and Functional Materials for Heavy Vehicle Applications

J. Sankar, Z. Xu, and Q. Wei
North Carolina A&T State University

Objective/Scope

The tasks of our work includes the following:

- To understand the high temperature mechanical performance (creep, fatigue) of self-reinforced silicon nitride ceramics;
- To understand the environmental effect on the high temperature mechanical behavior of self-reinforced silicon nitride ceramics;
- To understand the microstructures of the silicon nitride ceramics, and
- To understand the effect of surface engineering (coating) on the mechanical properties of silicon nitride and environmental effect on ceramic systems performance.
- To investigate the effect of Partially Stabilized Zirconia (PSZ) thermal barrier coating on diesel engine performance.
- To use Finite Element Methods (FEM) to understand the behavior of the various materials systems under investigation through modeling.
- To investigate the combustion chemical vapor deposition technique of fully stabilized zirconia thin films for solid oxide fuel cells

The research presented details the work carried out related to solid oxide fuel cells and includes three (3) major steps.

Step 1: Combustion Chemical Vapor Deposition Device Development -
Develop and design a combustion chemical vapor deposition device for the film processing.

Step 2: Experimental Parameters Optimization -
Conduct a series of parametric experiments (temperature of substrate, ratio of fuel components etc) to obtain a fully stabilized cubic phase zirconia films.

Step 3: Characterization of the Deposited Film -
Use Scanning Electron Microscopy (SEM) and X-ray Energy Dispersive System (EDS) to understand the quality of the deposited film against the processing parameters.

Technical Highlights

Zirconium oxide has been extensively used in tribological and thermal barrier coatings for many years. Among its most interesting properties is the ion conductivity in cubic or tetragonal phase. Therefore it can be used as oxygen sensor and electrolyte in solid oxide fuel cells (SOFCs). The cubic phase is preferred in SOFCs because of its highest oxygen ion conductivity. Yttria stabilized zirconia (YSZ) is one of the successful solution to obtain fully stabilized cubic phase. Moreover, to minimize the electrical path of fuel cell, thin film of the electrolyte is preferred.
Combustion chemical vapor deposition (CCVD) has been used to deposit thin films of diamond and many kinds of oxides, such as Al_2O_3, Cr_2O_3, SiO_2, and Yba2Cu3Ox (YBCO). It can also be used to process YSZ thin films. Among techniques to prepare the YSZ electrolyte thin film for

SOFCs, CCVD in the open atmosphere has potential to have high deposition rate and low operational cost.

Results and Discussion

We have established a liquid fuel CCVD system (Fig. 1). Basically, this system consists of a quaternary HPLC pump, an atomizer, pilot flame, and substrate cooling/holding supporter. The pump is used to deliver reagent solutions to a capillary atomizer. Aerosol is produced at the exit of the atomizer and ignited by the pilot flame. The reagents are then decomposed and some chemical reactions between the reagent radicals take place in the aerosol flame. Yttria stabilized zirconia (YSZ) thin film is expected to be deposited on substrate placed at the end of the aerosol flame.

Some preliminary experiments have been conducted with positive results. Zirconium 2-ethylhexanoate and yttrium 2-ethylhexanoate solved in toluene are used as reagents. Thin films are deposited on Si(100) substrates. The ratio of the fuel to oxygen is studied to obtain stable fully oxidized flame (Fig. 2) before any deposition experiment. Scanning electron microscopy (SEM) images in Fig. 3 show that the grain size of films is depended on the processing temperature. The films are also characterized with energy dispersive (Fig. 4) to identify the composition.

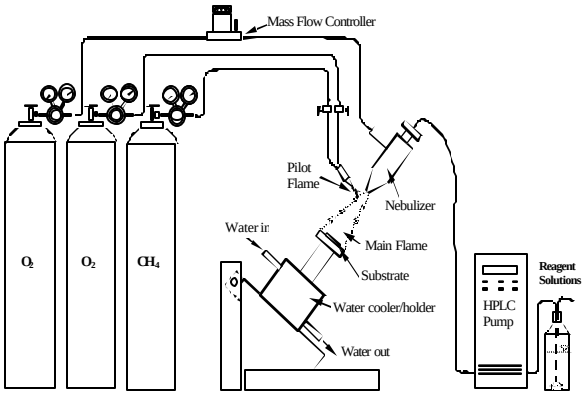

Fig.1. System of combustion chemical vapor deposition

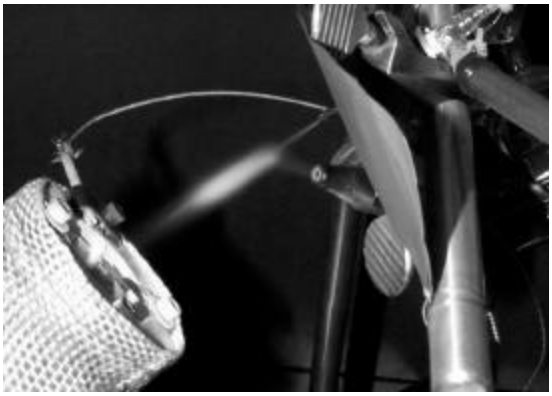

Fig. 2. Picture of the flame

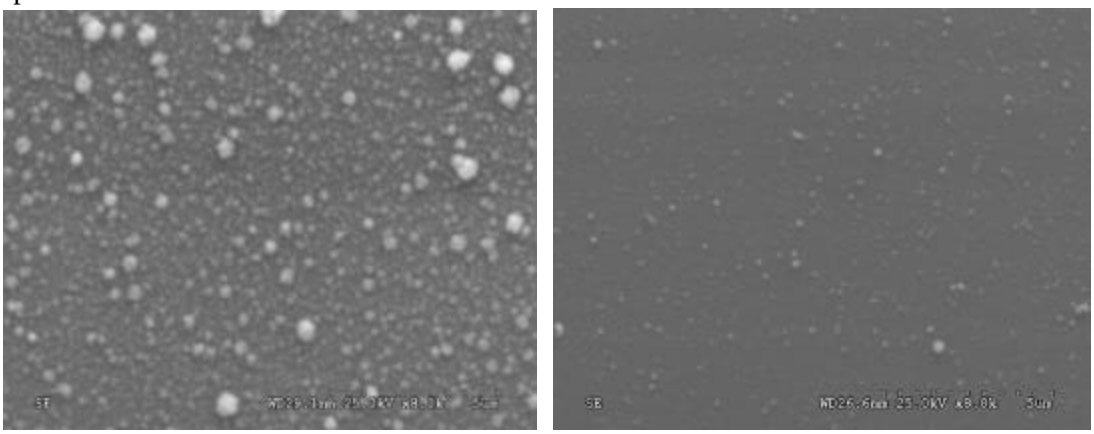

(a) (b)

Fig. 3. SEM images of the films deposited at different temperatures, a) at 900 ^{0}C, b) at 1200 ^{0}C.

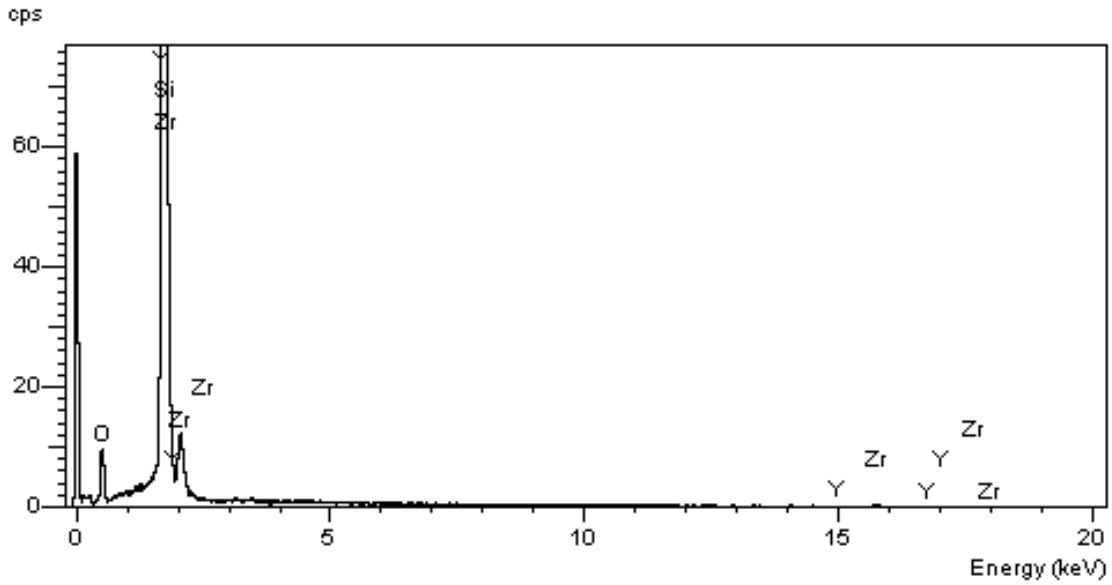

Fig. 4 EDS pattern of deposited YSZ film

Status of Milestones

On schedule.

Communications/Visitors/Travel

Dr. Ray Johnson visited the university and had discussion related to various research activities that are being carried out as part of this program

Publications

None.

Problems encountered

None.

Life Prediction of Diesel Engine Components

H. T. Lin, T. P. Kirkland, M. K. Ferber
Oak Ridge National Laboratory
and S. K. Lee and M. J. Andrews
Caterpillar Inc.

Objective/Scope

The valid prediction of mechanical reliability and service life is a prerequisite for the successful implementation of structural ceramics as internal combustion engine components. There are three primary goals of this research project which contribute toward that implementation: the generation of mechanical engineering data from ambient to high temperatures of candidate structural ceramics; the microstructural characterization of failure phenomena in these ceramics and components fabricated from them; and the application and verification of probabilistic life prediction methods using diesel engine components as test cases. For all three stages, results are provided to both the material suppliers and component end-users.

The systematic study of candidate structural ceramics (primarily silicon nitride) for internal combustion engine components is undertaken as a function of temperature (< 900°C), environment, time, and machining conditions. Properties such as strength and fatigue will be characterized via flexure and rotary bend testing.

The second goal of the program is to characterize the evolution and role of damage mechanisms, and changes in microstructure linked to the ceramic's mechanical performance, at representative engine component service conditions. These will be examined using several analytical techniques including optical and scanning electron microscopy. Specifically, several microstructural aspects of failure will be characterized:

(1) strength-limiting flaw-type identification;
(2) edge, surface, and volume effects on strength and fatigue size-scaling
(3) changes in failure mechanism as a function of temperature;
(4) the nature of slow crack growth; and
(5) what role residual stresses may have in these processes.

Lastly, numerical probabilistic models (*i.e.*, life prediction codes) will be used in conjunction with the generated strength and fatigue data to predict the failure probability and reliability of complex-shaped components subjected to mechanical loading, such as a silicon nitride diesel engine valve. The predicted results will then be compared to actual component performance measured experimentally or from field service data. As a consequence of these efforts, the data generated in this program will not only provide a critically needed base for component utilization in internal combustion engines, but will also facilitate the maturation of candidate ceramic materials and a design algorithm for ceramic components subjected to mechanical loading in general.

Technical Highlights

The dynamic fatigue test in four point bending on Kyocera SN235 and SN235P silicon nitride materials at 1000°C at stressing rates of 30 and 0.003 MPa/s was added to the test matrix reported previously and

completed during this reporting period, as indicated in Table 1. The objective of additional testing at 1000°C is to determine the transition temperature (thus, application limit) at which the materials exhibit a significant strength degradation and susceptibility to fatigue and/or creep. Both SN235 and SN235P silicon nitride bend bars were transversely machined per ASTM C116 standard. Results showed that SN235 and SN235P silicon nitride materials tested at 1000°C at 30 MPa/s exhibited a slight decrease in characteristic strength (4-5%) with respect to those obtained at 850°C at 30 MPa/s, as shown in Table 2. However, both SN235 and SN235P silicon nitride revealed a substantial loss in characteristic strength (44-46%) when tested at 1000°C at 0.003 MPa/s in air, as shown in Table 2 and Fig. 1. Note that previous report showed that SN235 and SN235P silicon nitride materials tested at 1200°C at 30 MPa/s and 0.003 MPa/s exhibited an extensive strength degradation due to the occurrence of creep deformation, evident by the permanent curvature of tested bend bars. The observed strength degradation at 1000°C at 0.003 MPa/s could be due to the onset of slow crack growth and/or creep processes, consistent with the low fatigue exponent obtained, as shown in Table 3 and Fig. 2. The present dynamic fatigue results suggest that the upper application limit temperature of both SN235 and SN235P is = 1000°C above which slow crack growth and/or creep processes will occur, resulting in a substantial degradation in mechanical strength and reliability. SEM analysis of fracture surfaces as well as polished cross sections of SN235 and SN235P silicon nitride specimens tested at 1000 and 1200°C will be carried out to elucidate the mechanical strength limiting and fatigue/creep processes.

Element mapping of Honeywell GS44 and Kyocera SN235 silicon nitride material after 1000 h exposure to an oil ash environment at 850°C in air is currently underway. The objective of the element mapping is to understand the effect of long-term oil ash exposure on the chemical composition of secondary phase(s) and the depth of materials influenced by the environment employed. The element mapping plus strength results could allow end users to predict the long-term stability and reliability of candidate silicon nitride materials under diesel engine environments.

A piece of Kyocera SN237 silicon nitride was acquired from S. K. Lee at Caterpillar to be included in the existing test matrix. The SN237 silicon nitride, presumably a more cost-effective material, was sintered with oxide sintering additives similar to those employed for SN235 and SN235P. Bend bars will be transversely machined per ASTM C116 standard. Dynamic fatigue tests will be carried out at 20, 850, and 1000°C at stressing rates of 30 and 0.003 MPa/s in air.

Status of Milestones

All milestones are on schedule.

Communications / Visitors / Travel

H. T. Lin presented a technical paper entitled "Comparison of Strength and Thermal Properties of Silicon Nitride Ceramics Up To 850C," A. A. Wereszczak, T. P. Kirkland, H. -T. Lin, and S. K. Lee, at the ASM Materials Solutions 2000 Conference, St. Louis, MO, October 9-12, 2000.

Dynamic fatigue results of SN235 and SN235P at 1000°C were communicated with S. K. Lee at Caterpillar.

Communication was made with S. K. Lee at Caterpillar regarding the proposal for the extension of the existing CRADA.

A piece of Kyocera SN273 silicon nitride was received from S. K. Lee to be included in the existing testing matrix.

Problems Encountered

None.

Publications

"High Temperature Inert Strength and Dynamic Fatigue of Candidate Silicon Nitrides for Diesel Exhaust Valves," A. A. Wereszczak, T. P. Kirkland, H. -T. Lin, and S. K. Lee, *Ceramic Engineering and Science Proceedings*, Vol. 21 (4), 497-508 (2000).

"Comparison of Strength and Thermal Properties of Silicon Nitride Ceramics Up To 850C," A. A. Wereszczak, T. P. Kirkland, H. -T. Lin, and S. K. Lee, was presented at the ASM Materials Solutions 2000 Conference, St. Louis, MO, October 9-12, 2000.

"Silicon Nitride Ceramic for Valve Train Applications in Advanced Diesel Engines," S. K. Lee, P. McCluskey, M. J. Readey, and H. T. Lin, to be presented at the 25th Annual International Conference on Advanced Ceramics and Composites," Cocoa Beach, FL, January 21-26, 2001

"Strength and Dynamic Fatigue of Silicon Nitride at Intermediate Temperatures," A. A. Wereszczak, H. -T. Lin, T. P. Kirkland, M. J. Andrews, and S. K. Lee, in preparation.

References

[1] A. A. Wereszczak, M. J. Andrews, M. K. Ferber, and T. P. Kirkland, "Life Prediction Verification," *Heavy Vehicle Propulsion System Materials Program Semiannual Technical Progress Report to DOE Office of Transportation Technologies*, Apr. 1997 - Sep. 1997.

[2] A. A. Wereszczak, and T. P. Kirkland, M. J. Andrews, M. K. Ferber, and R. Tandonl, "Life Prediction of Ceramic Diesel Engine Components," *Heavy Vehicle Propulsion System Materials Program Semiannual Technical Progress Report to DOE Office of Transportation Technologies*, Oct. 1998 - Mar. 1999.

[3] C. R. Brinkman, T. P. Kirkland, H. - T. Lin, R. A. Ott, S. K. Lee, and J. Thiele, "Life Prediction of Ceramic Diesel Engine Components," *Heavy Vehicle Propulsion System Materials Program Bimonthly Technical Progress Report to DOE Office of Transportation Technologies*, Apr. 2000 - May 2000.

[4] J. C. Cuccio, P. Brehm, H. T. Fang, J. Hartman, W. Meade, M. N. Menon, A. Peralta, J. Z. Song, T. Strangman, J. Wade, J. Wimmer, and D. C. Wu, *Life Prediction Methodology for Ceramic Components of Advanced Heat Engines, Phase 1*, DOE Report ORNL/Sub/89-SC674/1/V2, 1995.

Table 1. Silicon nitride test matrix to compare inert strength, high temperature fatigue performance, and effect of machining orientation. ASTM C1161B specimens are being 4-pt flexure strength tested

Test Condition	AS800	GS44	KYON 3000	KYON 3500	N7202	NT154	SN235	SN235P
20°C, 30 MPa/s Longitudinal	Completed	Completed	Completed		Completed	Completed	Completed	Completed
20°C, 30 MPa/s Transverse	Completed	Completed	Completed		Completed		Completed	Completed
500°C, 30 MPa/s Transverse		Completed						
500°C/ 0.003 MPa/s Transverse		Completed						
700°C, 30 MPa/s Transverse		Completed						
700°C 0.003 MPa/s Transverse		Completed						
850°C, 30 MPa/s Longitudinal	Completed	Completed	Completed		Completed	Completed	Completed	Completed
850°C, 30 MPa/s Transverse	Completed	Completed	Completed	Completed	Completed		Completed	Completed
850°C 0.003 MPa/s Longitudinal	Completed	Completed	Completed	Completed	Completed	Completed	Partially Completed	Completed
850°C 0.003 MPa/s Transverse	Completed	Completed	Completed	Completed	Completed		Completed	Completed
1000°C 30 MPa/s Transverse							Completed	Completed
1000°C 0.003 MPa/s Transverse							Completed	Completed
1200°C 30 MPa/s Transverse							Completed	Completed
1200°C 0.003 MPa/s Transverse							Completed	Completed
Material's Manufacturer	ASCC	ASCC	Kennametal	Kennametal	CFI	Norton	Kyocera	Kyocera

Table 2. Summary of uncensored Weibull strength distributions for Kyocera SN235 and SN235P silicon nitride specimens transversely machined per ASTM C1161.

Material	# of Spmns. Tested	Stressing Rate (MPa/s)	Temp. (°C)	Uncens. Weibull Modulus	± 95% Uncens. Weibull Modulus	Uncens. Chrctstic Strength (MPa)	± 95% Uncens. Chrctstic Strength (MPa)
SN235	15	30	20	23.8	15.4, 33.9	901	879, 923
SN235P	15	30	20	38.1	24.0 55.8	666	656, 676
SN235	15	30	850	26.7	18.0, 36.7	777	760, 793
SN235P	15	30	850	19.3	12.5, 27.6	631	612, 649
SN235	14	0.003	850	18.5	11.8, 26.8	744	720, 767
SN235P	15	0.003	850	18.2	11.5, 26.8	594	575, 612
SN235	15	30	1000	12	8.5, 17.2	711	686, 740
SN235P	11	30	1000	11	7.3, 17.1	560	536, 590
SN235	15	0.003	1000	20.6	14.5, 29.5	395	387, 405
SN235P	10	0.003	1000	22.8	14.7, 36.1	301	295, 309
SN235	9	30	1200	22.4	12.6, 34.8	442	427, 457
SN235	9	30	1200	61.3	34.5, 96.2	338	334, 342
SN235	6	0.003	1200	10.3	5.6, 16.7	247*	229*, 266*
SN235P	6	0.003	1200	18.5	9.0, 31.5	137*	130*, 145*

*Specimens crept-Shown rates/strengths uncorrected.

Table 3. Summary of uncensored dynamic fatigue exponents of Kyocera Si_3N_4.as a function of test temperature

Material	Machining Orientation	Temperature	Fatigue Exponent
SN235	Transverse	850	164
SN235P	Transverse	850	140
SN235	Transverse	1000	14
SN235P	Transverse	1000	13
SN235	Transverse	1200	14
SN235P	Transverse	1200	9

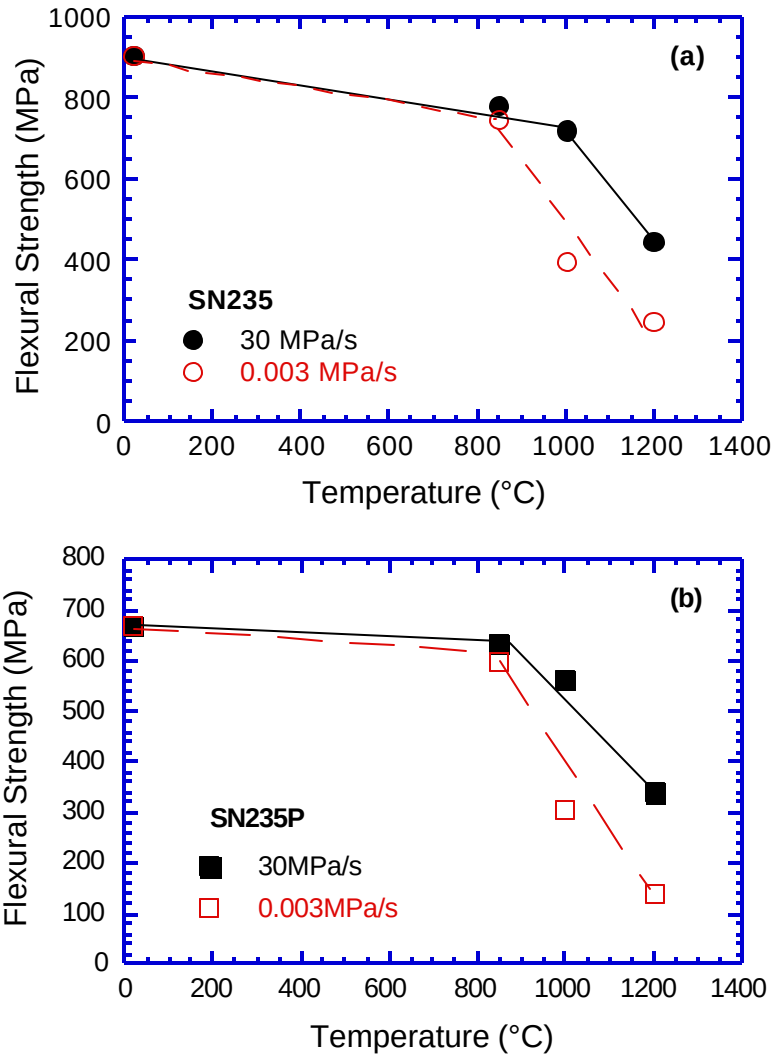

Figure 1. Strength versus test temperature curves of (a) SN235 and (b) SN235P tested under stressing rates of 30 and 0.003 MPa/s in air.

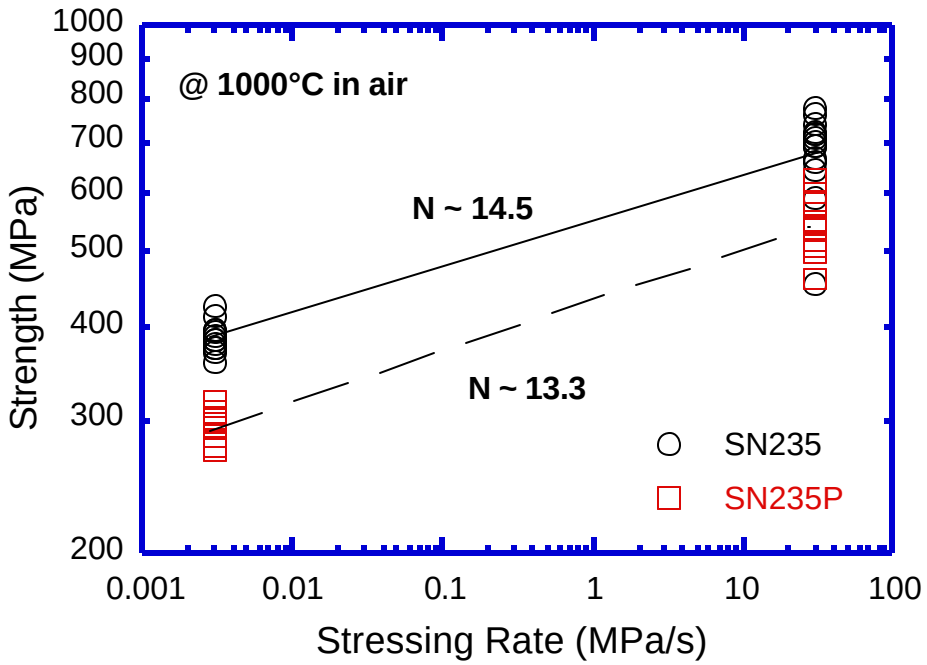

Figure 2. Strength versus stressing rate curves of Kyocera SN235 and SN235P tested at 1000°C in air.

Durability of Diesel Engine Component Materials

Peter J. Blau and Ronald D. Ott
Oak Ridge National Laboratory

Objective/Scope

The objective of this effort is to enable the development of more durable, low-friction moving parts in diesel engines for heavy vehicle propulsion systems by conducting friction, lubrication, and wear analyses of advanced materials, surface treatments, and coatings. The scope of materials and coatings is broad and includes any metallic alloy, intermetallic compound, ceramic, or composite material which is likely to be best-suited for the given application. Parts of current interest include valves, valve guides, and scuffing-critical components, like fuel injector plungers. Hot scuffing is a primary surface damage mode of interest. Bench-scale simulations of the rubbing conditions in diesel engine environments are used to study the accumulation of surface damage, and to correlate this behavior with the properties and compositions of the surface species. The effects of mechanical, thermal, and chemical factors on scuffing and reciprocating sliding wear are being determined, and the results will be used to refine material selection strategies for durability-critical engine components.

Technical Highlights

Completion and Testing of the High-Temperature Scuffing Apparatus. Construction of the high-temperature, oscillating scuffing test system was completed, and it was calibrated to measure frictional torque. As described in earlier reports, the basic geometric configuration consists of a horizontal, cylindrical specimen pivoting on a square, flat specimen beneath it. The lower specimen contains a 6.4 mm-diameter center hole to avoid the contact singularity at the pivot point. The upper specimen is driven by a rack and pinion gear arrangement and a slider-crank motor drive in line with a load cell to measure the pivoting torque. The pivoting torque is monitored to detect the on-set of surface damage, such as scuffing and scoring.

Specially-designed specimens and holders facilitate alignment of the contact. Alignment is important because the location of damage on the surfaces and the time to its on-set can be significantly affected by specimen alignment. The shape of the oscillating contact is suggestive of a bowtie, and thus, we decided to call this test method the "bowtie scuffing test."

When calibrating the apparatus, it was necessary to measure the inertia and intrinsic torque of the oscillating column so that the actual torque arising from scuffing contact could be determined. This measurement was performed in two ways: (1) by suspending the upper column by a high-tensile fiber and operating the gear drive while recording the load-cell signal, and (2) by pivoting the shaft on a lubricated ball and monitoring the load-cell signal. As described in more detail in the Milestone Report (under preparation), both methods gave similar results. This reference level drive-train torque reading was applied to experimental data to enable the separation of the sliding contact friction component from the total load-cell output.

The first series of tests was performed using Type 304 stainless steel flat specimens and cylindrical specimens of Type 303 stainless steel, Stellite 6B, and GallTough™ a specialty stainless steel. The lower specimens were ground and hand lapped on wet SiC paper of 600 grit in order to develop a

typical engineering surface finish and to facilitate the observation of surface damage on the test specimens. The upper test specimens were tested in the as-turned condition. Information on the surface finishes will be available in the Milestone report. All material combinations tested in the room temperature baseline series produced indications of arc-shaped scoring at the extrema of the cylinder specimens. Within several minutes of the on-set of sliding, a grinding noise could be heard.

Table 1 summarizes the results of preliminary experiments at room temperature under a normal force of about 12.54 N and speed of 0.98 cycle/sec. In several cases, tests were performed using graphite and 15W40 diesel oil to examine the torque response when the contact friction was reduced. Test lengths were kept relatively short because they were intended to check alignment and torque under minimal surface damage conditions. The higher friction of the GallTough and Stellite 6B cylinders on 304 suggests their tendency of these materials to begin to cut into the 304 stainless and raise the frictional torque. In fact a grinding noise was observed a few seconds into the tests on the latter materials.

Table 1.
Representative Torque and Friction Coefficient Data from the First Set of Bowtie Scuffing Tests
(the lower flat specimen was Type 304 stainless steel, 12.54 N load, 0.98 cyc/s, room temperature)

Cylinder Specimen Material	Lubricant	Test length (cycles)	Average Torque* (N-mm)	Friction Coefficient**
303 stainless steel	15W40 oil	30	12.35	0.12
303 stainless steel	graphite	30	36.19	0.18
303 stainless steel	none	20	39.72	0.40
GallTough stainless steel	none	100	78.75***	0.79
Stellite 6B	none	100	96.56***	0.97

* compensated for the zero-friction contact torque – average of two tests under these conditions
** calculated from the average torque and the location of the arcs of contact from the center pivot point
*** longer test length increased the level of damage and resulted in higher average torque readings

Two descriptions of the test method are in preparation. The first is contained in the project Milestone Report, and the second is a poster presentation that was submitted to the International Conference on Wear of Materials. A request was made to extend the delivery date for the Milestone Report until February 28, 2001, in order to complete the first elevated temperature series of tests. This delay may also require an extension of the March 31, 2001 milestone date for completion of tests of candidate materials and coatings.

Future Plans

1. Fabricate additional test specimens for elevated temperature scuffing tests and begin evaluating candidate materials for EGR applications.

2. Continue work on the design of a new testing system to evaluate the durability of fuel injector plungers.

Travel

On November 9, P. Blau joined a team of four other ORNL staff members on a visit to Honeywell Commercial Vehicle Systems in Elyria, Ohio, to discuss potential collaborations in the development of materials and designs for diesel engine components and braking subsystems.

On November 15-17, P. Blau co-chaired an ASTM Workshop on "Friction Test Methods for Research and Applications," in Orlando, Florida. This standards-related workshop was designed to describe the newest techniques for measuring friction in a spectrum of situations, ranging from micro-electromechanical systems (MEMS) to automotive brakes and aircraft tires on icy runways. Since Blau also chairs ASTM Committee G-2 on Wear and Erosion, he also conducted the semi-annual committee meeting that followed the workshop.

Status of Milestones

The following milestones were developed for FY 2001.

1) Complete baseline scuffing tests at room and elevated temperature. Submit report. (milestone date change to February 28, 2001 requested)

2) Complete elevated temperature scuffing tests of leading candidate materials and coatings. Submit report. (March 31, 2001 – extension is under consideration based on later completion of milestone (1) above)

3) Complete design and construction of a computer-controlled fuel injector materials testing system capable of studying the effects of varying injector motions and loading cycles on material response. (September 30, 2001)

Problems Encountered

Machining of the test specimens delayed the completion of the baseline high-temperature tests and may necessitate the adjustment of downstream milestone dates.

Publications and Presentations

P. J. Blau and R. D. Ott, "Development of a High-Temperature, Bowtie Scuffing Test for Diesel Engine Applications," submitted to the International Conference on Wear of Materials, Vancouver, BC, Canada, April 23-26, 2001.

Implementing Agreement for A Programme of Research and Development on Advanced Materials for Transportation Applications

M. K. Ferber
Oak Ridge National Laboratory

Objective/Scope

The International Energy Agency (IEA) was formed via an international treaty of oil consuming countries in response to the energy crisis of the 1970s. A major objective of the IEA is to promote secure energy supplies on reasonable and equitable terms. The governing board of the IEA, which is composed of energy officials from each member country, regularly reviews the world energy situation. To facilitate this activity, each member country provides energy experts who serve temporary staff assignments at IEA headquarters. These staff or secretariat support the governing board by collecting and analyzing energy data, making projections in energy usage, and undertaking studies on specialized energy topics. The governing board is also assisted by several standing groups; one being the committee on energy research and technology (CERT), which encourages international cooperation on energy technology. Implementing agreements (IAs) are the legal instruments used to define the general scope of the collaborative projects. There are currently 40 active implementing agreements covering research topics such as advanced fuel cells, coal combustion science, district heating and cooling, enhanced oil recovery, fluidized bed conversion, fusion materials, solar heating and cooling, pulp and paper, hydropower, heat pumping technologies, hybrid and electric vehicles, high temperature super conductivity, wind turbines, and high temperature materials. A complete listing can be found at the IEA website, www.iea.org.

This progress report summarizes recent activities in the implementing agreement entitled, "Implementing Agreement For A Programme Of Research And Development On Advanced Materials For Transportation Applications." This implementing agreement currently consists of one active annex entitled," Annex II: Co-Operative Program on Ceramics for Advanced Engines and Other Conservation Applications". The motivation for this IA is the development of new and improved ceramic materials, brittle material design methods, and life prediction methodology. The objective of Annex II is coordinated R&D on advanced ceramics leading to standardized methods for testing and characterization. The participants wish to avoid unnecessary duplication of research efforts and to accelerate the achievement of their R&D program objectives. International Standards energize industrial activity, employment, and international trade.

Technical Highlights

Annex II currently consists of one active effort, Subtask 11. In this subtask, techniques for the measurement of thermal and mechanical fatigue are being examined. National efforts in Japan and the United States focus on the development of procedures for evaluating the mechanical fatigue behavior of silicon nitride ceramics using either uniaxial flexure or biaxial test specimens. The national effort in Germany consists of the development of thermal fatigue procedures using the laser thermal shock equipment

evaluated in Subtask 9. The national effort in Sweden will focus on the evaluation of the fracture surfaces of specimens tested in Japan, the United States, and Germany.

Subtask 11 will also include an international effort in which the thermal fatigue behavior of a single silicon nitride will be compared with the mechanical fatigue data generated at a temperature which is the same as that at the fracture point in thermal fatigue test. Germany will be responsible for the thermal fatigue testing while both Japan and the United States will conduct mechanical fatigue testing. Sweden will perform fractographic analysis of the specimens.

The preliminary fatigue testing of a structural silicon nitride ceramic in Japan has revealed little or no cycle dependent strength degradation at temperatures at least 1000°C. In the United States, specimens for rotary bend fatigue have been machined and will be tested during the next reporting period.

Status of Milestones

All milestones are on track.

Communications/Visits/Travel

None

Publications

None

References

None

Standards For Reliability Testing Of Heavy Vehicle Propulsion Materials

Said Jahanmir, James F. Kelly, and William Luecke
National Institute of Standards and Technology

Objective/Scope

The objective of this project is to develop international standard test methods for assessing the reliability of ceramic components used in diesel engines and other heavy vehicle propulsion systems. Advanced ceramics such as silicon nitrides offer unique combination of properties that include light-weight, high-temperature strength, and resistance to wear and corrosion. These properties make them particularly attractive for diesel engines where their use as key engine components will allow the higher operating temperatures that lead to higher thermal efficiencies and environmentally cleaner propulsion systems. Reliability and cost-effectiveness are critical issues in implementing ceramics in the valve train of diesel engines. Ceramic valve train components are subjected to demanding conditions that include high contact loading, elevated temperatures, and corrosive environments. To ensure a reliable service life, standard test methods are needed to evaluate the performance of potential ceramics in highly loaded rolling and sliding contacts. This project will develop test methods for evaluating the contact fatigue behavior of ceramics under rolling and sliding conditions that simulate the cam roller followers, valves and valve seats. In support of this goal we will pursue four research thrusts. We will evaluate the effect of machining damage on contact reliability as well as the interactions between machining and contact damage that may lead to premature failure. The project will also consider fundamental issues in the relation between ceramic microstructure and performance reliability. Finally, we will investigate the basic mechanisms that lead to formation and propagation of contact damage and the effect on reliability of residual stresses developed during machining and by contact.

Technical Highlights

Recently NIST has lead several IEA international round robin studies to establish the repeatability and reproducibility of test methods for the characterization of ceramic powders. This effort has lead to the establishment of several standard test methods both in the U. S. and the IEA collaborating countries. Due to the interest in the Heavy Vehicle Propulsion System Materials Program on the development of international standard methods for characterization and testing of advanced materials for diesel engines, the powder characterization project has been transferred to the Versailles Project on Advanced Materials and Standards (VAMAS). This transfer is a natural step towards development of international standard test methods for advanced materials. Within the Heavy Vehicle Propulsion System Materials Program we plan to initiate a new activity focused on test methods and standards for assessing the reliability of advanced materials used for diesel powered heavy vehicles.

During FY 2000 thirty-four laboratories from Belgium, Germany, Japan, Sweden and the U.S. completed an international round robin study on properties of advanced ceramic powders. The goal of this activity, conducted under the auspices of the International Energy Agency (IEA), is to draft uniform standard test methods in each participating country and through the ISO. The

participants measured properties including those used for characterizing powders suspended in water (e.g., particle dispersion and rheology), for characterizing spray dried powders (e.g., flow rate, particle size distribution, and moisture and binder content), and for evaluating green bodies (e.g., bulk density and green strength). Each laboratory used the same pre-defined procedure for each measurement. Analysis of the data for within- and between-laboratory repeatability demonstrated that, in general, there were no significant problems within the laboratories. However, there were significant variations between laboratories for a few measurement methods. The measurement methods that resulted in unacceptable variation must be evaluated further to improve the procedures used for testing before the results can be used to establish national and international standard test methods.

This activity will continue as IEA Subtask 12. The consensus of the participating laboratories through mail and email surveys was to concentrate this year on completion of the extension of the moisture/binder content measurement procedures for spray dried granules, and transfer the other powder characterization projects to VAMAS. They agreed to a work plan for IEA Subtask 12 for measuring moisture and binder content, using alumina granules provided by the Japanese participants. The material and the testing protocols were distributed to the participating laboratories in the U.S., Germany, Japan, Belgium, and Sweden for round robin testing. The U.S. and German laboratories have completed the measurements of moisture and binder content, and results from the Japanese participants are expected in February. The laboratories in Sweden and Belgium have chosen not to participate in this activity.

The following testing protocol for characterization of moisture content and binder content was distributed to the participants.

<u>Note; please use three powder samples, and perform this procedure once for each</u>
(1) Moisture Content Measurement Procedure:

Equipment:
- Oven: an oven capable of reaching a temperature of 150 °C
- Balance: a balance suitable for weighing to 1 mg
- Balance bottle: a glass balance bottle

<u>Note; Start this measurement as soon as you open the bottle.</u>

a) Weigh the clean container with cap (balance bottle)
b) Place a 10 g sample in the container and measure the total mass (container with cap +sample). (<u>A bottle has about 10 g</u>)
c) Dry the container at 105±1 °C for 2 h. Put the cap on the container, but keep opening space.
d) Cover it with the cap and move it to desiccator to cool it to room temperature.
e) Weigh the total mass of the container and sample. (do not remove the cap)
f) Repeat the steps until the weight change becomes less than 5 mg. Use 1 hour drying time for the repeat steps.
g) Record temperature and relative humidity.

Calculate the moisture content according to the following equation:

Moisture content =(W1-W2)/(W1-W3) × 100
W1: (sample + container + cap) before drying
W2: (sample + container + cap) after drying
W3: (container + cap)

(2) Binder Content Measurement Procedure:

Equipment:
Balance: a balance suitable for weighing accurately 1mg;
Furnace;
Crucible

Note: After the moisture content measurement, use the same powder samples for the binder content measurement.

a) Weigh the crucible (W3)
b) Place the powder sample in the ceramic crucible and weigh the crucible with powder (W1)
c) Heat the sample in the furnace in air 5 °C/min to 500 °C and keep it there 1 h.
d) Cool the crucible with sample in a desiccator to room temperature and weigh it (W2).
e) Record room temperature and relative humidity.

Calculate the moisture content according to the following equation:

Moisture content =(W1-W2)/(W1-W3) × 100
W1: (sample + crucible) before drying;
W2: (sample + crucible) after drying;
W3: crucible

Figures 1 and 2 show the preliminary results of the testing for moisture content and binder content. Although complete statistical analysis will await the results from Japan, it is apparent that the interlaboratory variability is much greater than the intralaboratory variability for the binder content.

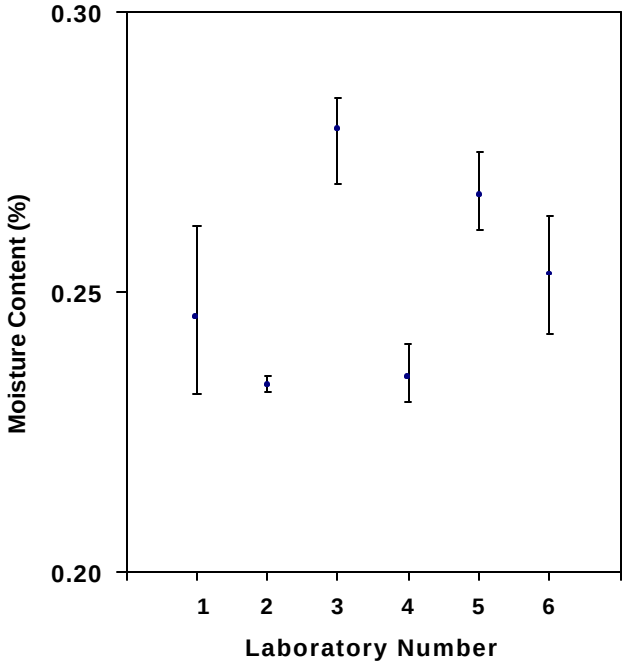

Figure 1. Results of moisture content measurements on alumina powder samples. The graph shows the maximum, minimum, and average values from each of the six laboratories that have reported to date.

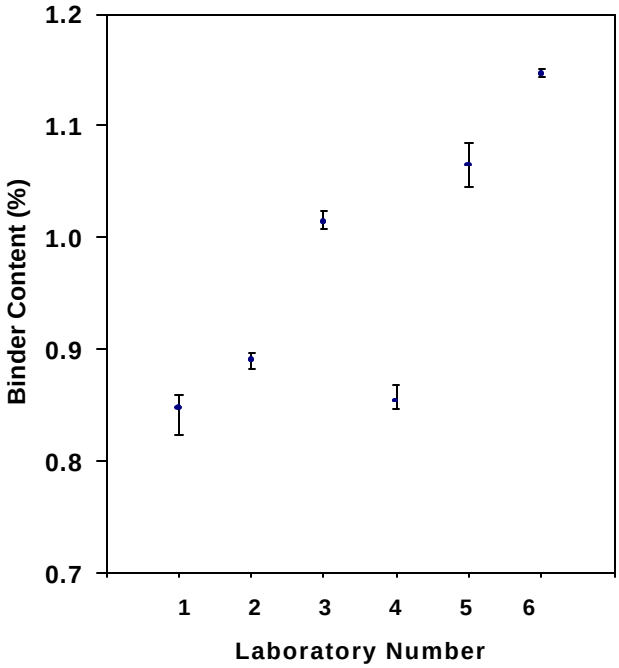

Figure 2. Results of binder content measurements on alumina powder samples. The graph shows the maximum, minimum, and average values from each of the six laboratories that have reported to date.

To develop plans for the new FY 2001 project on reliability, we have contacted several diesel engine companies and their material suppliers to assess their interest in participating in a new project on test methods and standards for assessing reliability of advanced materials used for diesel powered heavy vehicles. Everyone has expressed a keen interest in the new project and has offered to collaborate and participate, either by providing ceramics or conducting round-robin testing. We are planning a meeting at NIST with industrial partners in late April or early May to jointly develop a detailed work plan. We are initiating the testing program by evaluating the feasibility of using a commercial rolling contact fatigue (RCF) tester that is available at NIST and at the laboratories of several potential partners.

Status of Milestones

1. Complete final report for the first year effort on Subtask 12 (December 30, 2000) – Delayed
2. Initiate a new project direction and develop collaboration with diesel engine companies in the U.S. and IEA countries (February 28, 2001) – on schedule
3. Evaluate feasibility of possible test methods for standardization (September 30, 2001) – on schedule

Communication/Visits/Travel

We have contacted several diesel engine companies and their material suppliers to assess their interest in participating in a new project on test methods and standards for the assessment of reliability of advanced materials used for diesel powered heavy vehicles.

Publications

None

References

None

Mechanical Property Testing and Standards Development

George Quinn
National Institute of Standards and Technology

Objective/Scope

This task is to develop mechanical test method standards in support of the Propulsion Systems Materials Program. Test method development should meet the needs of the DOE engine community but should also consider the general USA structural ceramics community as well as foreign laboratories and companies. Draft recommendations for practices or procedures shall be developed based upon the needs identified above and circulated within the DOE ceramics engine community for review and modification. Round robins will be conducted as necessary. Procedures will be standardized by ASTM and/or ISO.

Technical Highlights

1. General

In this quarterly period, attention was focused on refinements to fracture toughness testing. An ASTM Symposium on Fracture Resistance Testing was held in November 2000. Major revisions to the fracture toughness standard C 1421 are being prepared for ASTM ballot.

2. Fracture Toughness

a. ASTM standard and NIST SRM 2100

The ASTM standard for fracture toughness C 1421 was completed in 1999. We now are making a series of papers and presentations on it in order to inform the ceramic and engine communities about the standard. Three papers were prepared for the symposium on Fracture Resistance Testing at Orlando in November 2000 in connection with the ASTM Committee C-28 meeting. This conference was co-organized by Mr. Quinn, J. Salem of NASA-Glenn, and M. Jenkins of the University of Washington. The purpose of the conference was to highlight standard C 1421, the new Standard Reference Material that supports it, and review current issues pertaining to fracture testing of ceramics. Sixteen papers were presented by various authors and will be published in a new ASTM Special Technical Publication. Mr. Quinn prepared and presented two papers for the symposium: one on SRM 2100 and one of the five Versailles Advanced Materials and Standards

round robins on fracture toughness testing which featured over 4,500 experiments! A third coauthored paper was coordinated by M. Jenkins and was on C 1421 itself.

b. New Experiments, SCF method, Sintered Alpha Silicon Carbide

In the course of preparing C 1421, we compared fracture toughness outcomes from the three methods to verify that consistent results could be obtained. Indeed, extraordinarily consistent results were obtained by the surface crack in flexure (SCF), Single-Edged Precracked Beam (SEPB), and Chevron Notch in Bending (CNB) methods for the hot-pressed silicon nitride NC 132 that comprised the reference material SRM 2100. Good correlations were noted for alternative materials, but we were puzzled by minor 5-10% discrepancies in the fracture toughness outcomes reported for Carborundum's sintered alpha silicon carbide (Hexaloy SA). Various groups, using the three methods in C 1421, had obtained between 2.5 and 3.1 MPa√m over the last 20 years. Some of the variability is undoubtedly due to minor variations in the test procedures that had not been standardized. Other variability was due to batch-to-batch differences in this material, which is pressure less sintered. It sometimes can have small density or silicon carbide grain morphology differences from lot to lot. At NIST through the years, we have evaluated several batches of this material and obtained SCF fracture toughness values of 2.7 to 3.0 MPa√m. Recent work at NASA-Glenn with the SEPB and CNB methods has been producing somewhat lower outcomes: 2.4 to 2.7 MPa√m.

We therefore agreed to test some NASA CNB specimen fragments by the SCF method at NIST in order to obtain a direct comparison. Six specimens designated "II-UW #1-6" were Knoop precracked at NIST using a 49 N (5 kgf) load as prescribed in C1421. The indentation and residual stress damage zone were hand ground away in accordance with C 1421 with one important exception described now.

During the hand polishing, the specimens were periodically examined to detect whether lateral cracks were present. The goal of the SCF method is to produce a nice, primary, semi elliptical median type crack without interference of residual stresses or any other artifacts. In recent years, we have become aware that <u>lateral</u> cracks may extend very deep beneath the Knoop indentation in some materials. Even after hand grinding or polishing off the requisite 4.5 to 5 times the indentation depth to remove the residual stresses, vestigial lateral cracks may still be present and may shield the main crack during subsequent loading to fracture. One consequence of the shielding effect is that a greater load must be applied to the test piece to fracture it, than would otherwise be the case if the median crack were unshielded. Hence, the calculated fracture

toughness by the SCF method could overestimate the true fracture toughness. This could explain why the SCF results are often a little (5-10%) greater than comparable SEPB or CNB outcomes.

We learned that vestigial lateral cracks did indeed penetrate deeply beneath the surface in the sintered silicon carbide. Their last traces were eliminated only after 7 to 10 times the indentation depth of material was removed. After this step, the 3 mm x 4 mm x ~25 mm specimens were broken in four-point flexure using 10 mm x 20 mm fixtures. The outcomes of the experiments are listed in Table 1, along with the chevron notch outcomes obtained on the identical test pieces. The agreement is excellent. In fact, the best agreement was obtained with the first four specimens which had the greatest amount of material removed by hand polishing.

Table 1. Fracture toughness results for sintered alpha silicon carbide specimens. The SCF specimens were halves of the same CNB specimen. Thus, for example, specimen #1 produced a CNB toughness of 2.71 MPa√m and a remnant half of that same specimen produced an SCF toughness of 2.67 MPa√m.

Specimen	$K_{I, CNB}$ Chevron Notch in Bending MPa√m	$K_{I, SCF}$ Surface Crack in Flexure MPa√m	Amount of material removed, SCF method*
1	2.71	2.67	10.4 h
2	-	2.69	9.3 h
3	2.57	2.57	10.9h
4	2.59	2.64	8.4 h
5	2.60	2.79	6.2 h
6	2.61	2.76	7.1 h**
average	2.62	2.69	
std. dev.	.06	.08	

* h is the depth of the Knoop indentation. C 1421 specifies only 4.5 to 5.0h should be removed.
** A trace of the lateral crack trace was still present

Thus, we may have detected a small glitch in the SCF procedure and, as this is being written, several hundred previously tested SCF specimens are being examined of vestigial laterals. The inspection procedure is very simple. The tensile surfaces of the fractured test pieces are examined for tell tale pullouts or chip outs in the vicinity of the Knoop precrack. Hand polishing or grinding tends to create pullouts from the lateral cracks if they are present. Vestigial lateral cracks have

only been detected in a handful of very brittle ceramics or glasses and most of our enormous SCF database is unaffected by this problem.

We will propose that the SCF method be revised slightly in C 1421. The remedy is quite simple: after hand polishing 4.5 to 5.0 times the indentation depth away to remove the residual stresses, examine the tensile surface with a low power optical microscope at 20X to 100X. If vestigial laterals are present, then hand grind a little deeper prior to fracturing the specimen.

c. New planned SCF experiments

A large batch of new specimens has been prepared and will be tested in early 2001. The new specimens will be tested with the following objectives in mind:

1. Test another batch of alpha silicon carbide specimens to confirm the lateral crack problem identified above.
2. Test several materials already evaluated by NASA with the SEPB and CNB methods.
3. Test Ceradyne SRBSN specimens to correlate results to the comprehensive machining damage study just concluded, and also to attempt to measure an R-curve via the SCF method.

d. Revisions to C 1421

We have identified a number of minor editorial mistakes, unclear sections, or topics that needed improvement in ASTM standard C 1421. Rather than correct the document piecemeal, the task group decided to roll up as many changes as possible at one time. In early January, the task group pooled their recommended changes and sent them to Mike Jenkins at University of Washington for an ASTM ballot in the spring of 2001. At least 35 changes will be proposed, ranging from minor rewordings to the following major changes:

1. Standard Reference Material 2100 will now be included as a means of verification. Precision and Bias section of the standard will be revised. Users will now be able to verify that they are conducting the tests properly and they can verify the accuracy and precision of their measurements. This will be the first fracture toughness test standard method in the world that is so supported.
2. Extra tips on conducting the SCF method will be included, with the goal of making the method easier to perform. For example, in some transparent materials it is very difficult to discern the Knoop precracks. A simple but effective expedient is to use an ordinary felt tip marker pen with green colored ink to paint the fracture surface. In many materials, the precrack is highlighted and is easy to see with an optical microscope at low power.
3. A warning about the lateral crack problem (described above) will be included.
4. The new alpha silicon carbide data will be included/.

5. Alignment of SEPB precracks in the 3-point fracture mode is revised and made simpler to accomplish.
6. Interpretation of slow crack growth halos around SCF precracks is clarified by reference to the work of Quinn and Swab.
7. Correction factors for chamfers in the SCF method will be included as a new annex.

Finally, we have proposed that a brief annex on the use of the SCF method to estimate R-curves has been proposed for inclusion, but the task group has yet to agree on this.

3. Flexure Testing of Cylindrical Ceramic Specimens

The paper on the analysis of the almost 200 fractured rods and bars of Ceradyne sintered reaction bonded silicon nitride for the July 2000 conference on fractography of Glasses and Ceramics was revised. The machining crack schematic drawings, Figures 1 and 2, that were prepared as a result of this work were turned over to Dr. Lewis Ives at NIST for inclusion in his new draft ASTM Standard Test Method for Effect of Surface Grinding on Flexure Strength of Advanced Ceramics.

4. Other

a. Design of new Semi articulating flexure fixtures for rectangular specimens

No activity this period

b. ISO TC 206, Working Group 16, Fracture Toughness by SCF method

No progress this period.

c. ISO TC 206, Working Group 2, Flexure Strength at Room Temperature

The draft standard passed the Final Draft International Standard ballot. The document has been approved an ISO standard.

d. ISO TC 206, Working Group 8, Flexure Strength at Elevated Temperature

The revised draft was prepared by the Japanese secretariat. It incorporates all requested revisions, including the new annex on the results of the VAMAS Technical Working Area 3 international round robin .was completed during this bimonthly period.

e. Modify ASTM Standards C 1198 and C 1259 for Elastic Modulus by Resonance

Revisions to standard C 1198 and C 1259 were prepared and sent to ASTM for a formal ballot in the spring of 2001. The revisions to the two standards are an appendix that includes a simple correction factor for elastic modulus if the beam specimens have chamfered edges such as in a flexural strength bar.

Status of Milestones

Milestones are being revised. Diametral compression testing is on hold pending completion of other tasks.

Communications/Visits/Travel

Data was exchanged with Jon Salem at NASA-Glenn on evaluating the fracture toughness of sintered silicon carbide and refining ASTM C 1421.

A set of references on the topic of whether Region II and III slow crack growth regimes (from K-V curves) could affect dynamic fatigue data interpretation was sent to J. Salem of NASA-Glenn. A typical dynamic fatigue analysis determines the slow crack growth exponent, N, but assumes that all crack growth occurs in Region I. In reality, at higher loading rates, regions II and II can alter the dynamic fatigue response.

Mr. Quinn attended the ASTM Committee C-28 meeting in Orlando and presented progress on several topics in subcommittee C28.01 (Properties and Performance) and C 28.94 (ISO TAG).

Mr. Quinn co-organized the ASTM Symposium on Fracture Resistance Testing in Orlando in November 2000.

Publications

1. M. Jenkins, G. D. Quinn, J. A. Salem, I. Bar-On, "Development, Verification and Implementation of a National Full-Consensus Fracture Toughness Test Method Standard for Advanced Ceramics," to be publ. in *Fracture Resistance Testing of Monolithic and Composite Brittle Materials, ASTM STP 1409,* J. A. Salem, M. G. Jenkins, and G. D. Quinn, eds., ASTM, West Conshohocken, PA 2001.
2. G. D. Quinn, "The Fracture Toughness Round Robins in VAMAS: What We Have Learned," *idem*.
3. G. D. Quinn, K. Xu, R. J. Gettings, J. A. Salem, and J. J. Swab, "Does Anyone Know the Real Fracture Toughness? SRM 2100: the World's First Ceramic Fracture Toughness Reference Material," *idem*.

References

None.

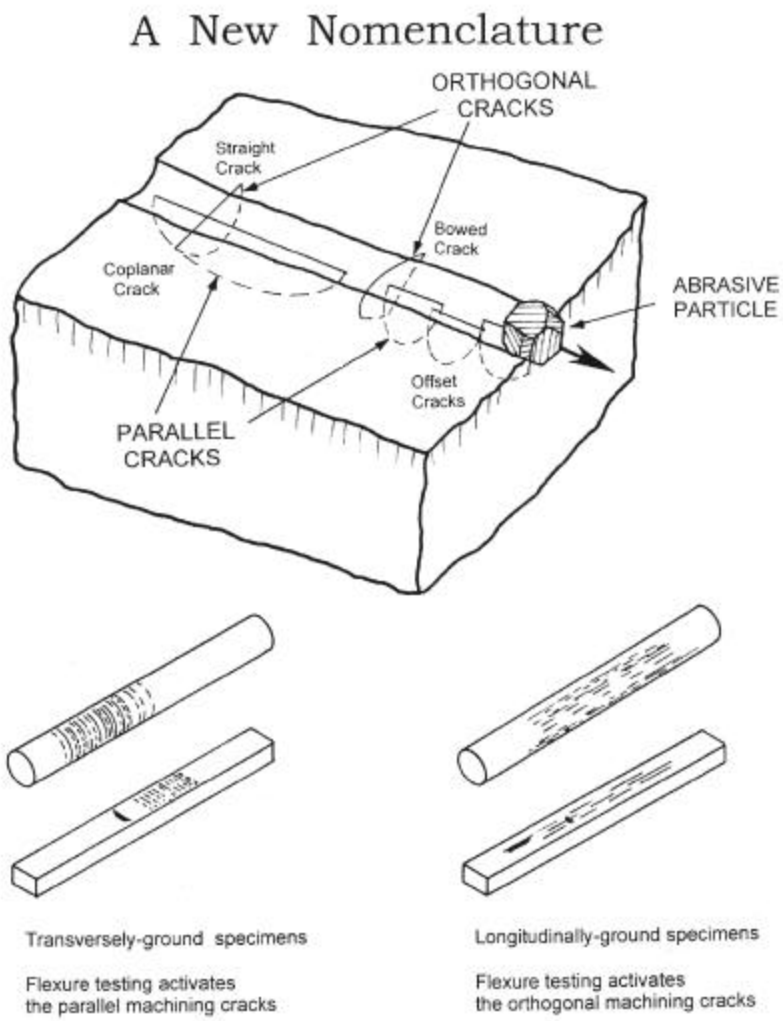

Figure 1. A new schematic drawing illustrating the type of subsurface cracks that may form as a result of surface grinding. This illustration is adapted from and includes corrections to an illustration originally prepared by Rice and Mecholsky in 1979.

Fractographic Manifestations of Machining Damage

GROUND SURFACES

Common in biaxial disks and *transversely-ground* uniaxial flexural or tension strength specimens.

(a) **elongated "coplanar parallel crack"**
(or coplanar linked semi-elliptical cracks).
A deep striation may or may not necessarily be present.
The fracture mirror may be **elongated** along the outer specimen surface.

(b) **elongated "coplanar parallel crack"**
linked with a **natural flaw**.
A step in the fracture origin emanates from the discontinuity.

(c) **"zipper crack"**
This is a series of short semi elliptical cracks, which have linked. A series of short tails, or **"machining crack hackle,"** emanate from the links or overlaps of the flaws and extend up into the fracture mirror. These tails may be tilted to the left or right and help confirm that fracture originated in the central region of the set. The short tails are telltale features of slightly misaligned or overlapping transverse machining cracks (or a scratch) and are often easier to see with an optical microscope with low angle lighting than with a scanning electron microscope. The fracture mirror may be elongated along the specimen outer surface or it may have one or two prominent **side lobes**.
This origin type is common in transversely-ground rectangular flexure specimens or scratched biaxial disk specimens.

(d) **coarse "zipper crack"**
This is made up of a series of irregular, less coplanar semi-elliptical cracks. Larger tails than in (c) are created. In severe cases, the tail may extend all the way to the mirror boundary. The fracture mirror may be elongated. This origin is common in transversely ground or scratched specimens and the markings are sometimes termed "shark's teeth."

(e) **"V machining crack"**
The crack(s) that intersects the fracture surface at an angle. Only a portion of the machining crack series is exposed. A pronounced step occurs in the fracture mirror. One or two (shown) tails extend well up into the fracture mirror. The machining direction is not quite perpendicular to the specimen length and uniaxial stress axis due to grinding wheel cross feed. This origin is common in cylindrical specimens prepared by centerless or transverse grinding wherein the wheel and work piece displace axially relative to each other.

Figure 2. Schematic of machining cracks in transversely ground ceramic specimens. The machining cracks leave tell tale features that help in their identification